arXiv:1111.6950v1 [quant-ph] 29 Nov 2011

Tensor networks and graphical calculus for open quantum systems

Christopher J. Wood,[1, 2, *] Jacob D. Biamonte,[3, 4] and David G. Cory[1, 5, 6]
[1]*Institute for Quantum Computing, Waterloo, ON, Canada*
[2]*Department of Physics and Astronomy, University of Waterloo, Waterloo, ON, Canada*
[3]*Centre for Quantum Technologies (CQT), National University of Singapore*
[4]*ISI Foundation, Torino Italy*
[5]*Perimeter Institute for Theoretical Physics, Waterloo, ON, Canada*
[6]*Department of Chemistry, University of Waterloo, Waterloo, ON, Canada*
(Dated: November 30, 2011)

We develop a graphical calculus for completely positive maps and in doing so cast the theory of open quantum systems into the language of tensor networks. We tailor the theory of tensor networks to pictographically represent the Liouville-superoperator, Choi-matrix, process-matrix, Kraus, and system-environment representations for the evolution of open-system states, to expose how these representations interrelate, and to concisely transform between them. Several of these transformations have succinct depictions as wire bending dualities in our graphical calculus — reshuffling, vectorization, and the Choi-Jamiołkowski isomorphism. The reshuffling duality between the Choi-matrix and superoperator is bi-directional, while the vectorization and Choi-Jamiołkowski dualities, from the Kraus and system-environment representations to the superoperator and Choi-matrix respectively, are single directional due to the non-uniqueness of the Kraus and system-environment representations. The remaining transformations are not wire bending duality transformations due to the nonlinearity of the associated operator decompositions. Having new tools to investigate old problems can often lead to surprising new results, and the graphical calculus presented in this paper should lead to a better understanding of the interrelation between CP-maps and quantum theory.

I. INTRODUCTION

A complete description of the evolution of quantum systems is an important tool in quantum information processing (QIP). In contrast to closed quantum systems, in open quantum systems the evolution need no longer be unitary. In general the evolution of an open quantum system is called a *quantum operation* or *quantum channel* which, for a discrete time interval, is described mathematically by a *completely positive map* (CP-map) [1].

In the context of QIP, a quantum channel is a completely positive linear map acting on the density operators which describe a physical systems state. A map $\mathcal{E}$ is *positive* if and only if it preserves the positivity of an operators spectrum, and *completely positive* if and only if it further satisfies the condition that the composite map $\mathcal{I}\otimes\mathcal{E}$ is positive, where $\mathcal{I}$ is the identity map on a space of density operators of at least equal dimension as the space on which $\mathcal{E}$ acts. We will consider the case when $\mathcal{E}$ is also *trace preserving*, which is to say $\mathrm{Tr}[\mathcal{E}(\rho)] = \mathrm{Tr}[\rho]$ for all density operators ρ. Since quantum systems are described by density operators, positive operators ρ with unit trace, the requirements that $\mathcal{E}$ be complete-positive and trace-preserving ensures that our output state will always be a valid density operator. Such maps are called completely positive trace preserving maps (CPTP-maps).

There are numerous representations for completely-positive maps, and while these representations are at least in principle equivalent, transformations between representations is often cumbersome and tedious. Thus a key result in the present paper is to introduce and develop graphical calculus methods that facilitate an intuitive unification and interoperability between these representations, the outcome of which is depicted in Fig. 1.

The graphical calculus casts the theory of open quantum systems into the framework of *tensor networks*, which comes equipped with a graphical means to represent and reason about the contraction of sequences of tensors [2]. Graphical calculi have been used to great benefit in several areas of modern physics with the most prolific example being the use of Feynman diagrams to calculate scattering amplitudes in quantum field theories [3]. In the case of tensor networks, their use dates back to earlier work by Penrose who's graphical notation is a useful starting point [2]. Recent work has been done on uniting the theory of tensor network states with modern algebra and similar graphical tools which have recently received interest in the quantum information, foundations and condensed matter communities [4, 5]. They have been used as computational tools for simulating many-body quantum systems efficiently [4, 6–8], as a tool for manipulating tensor networks and to generalize quantum circuits [5], and for exploring the foundations of quantum mechanics [9–12].

Although it is straightforward to translate equations into so called tensor string diagrams, a missing piece has been a graphical calculus for open systems theory which provided new results, and hence enhanced the potential for diagramatic reasoning. Several proposed graphical languages have been based on category theory or a generalization of quantum circuits [3–5, 13, 14]. Our work differs from the current approaches. We develop a calculus and tailor the tensor string diagrams of Penrose to

---

[*] christopher.j.wood@uwaterloo.ca

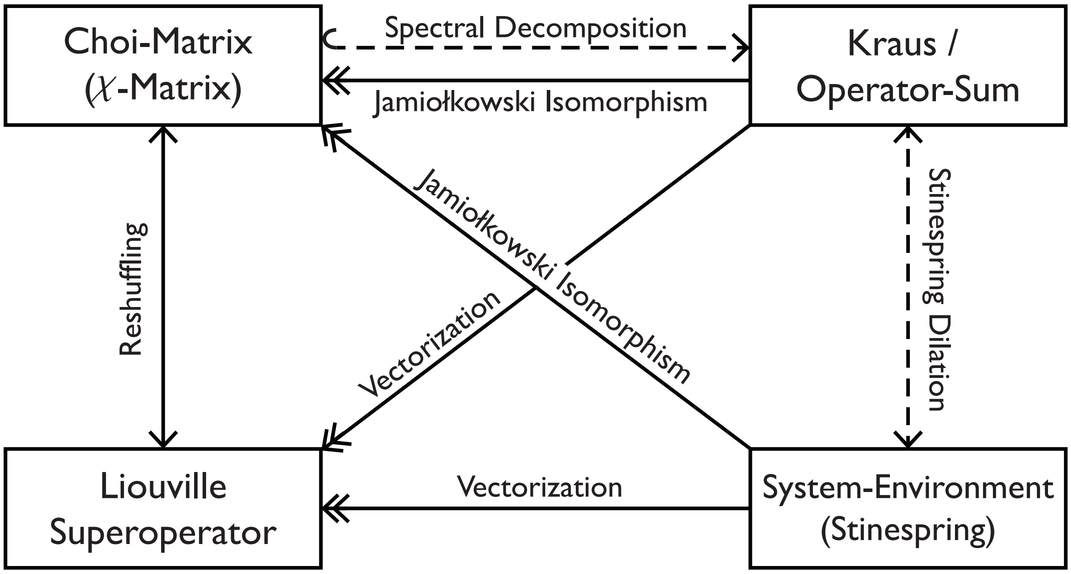

FIG. 1. The main mathematical representations for completely positive maps and how one may transform between them. Solid arrows represent linear operations which we prove can be done by "wire bending" transformations in our graphical calculus. Dashed arrows represent non-linear transformations. Reshuffling and Stinespring dilation are bijective transformations, vectorization and the Jamiołkowski isomorphism are surjective transformations, and the spectral decomposition is an injective transformation.

unify several mathematical representations used in open quantum systems and to transform freely between them. In accomplishing this, we express our graphical tensor calculus in the Dirac notation familiar in QIP instead of the abstract index notation used by Penrose. We have also introduce a graphical colour summation convention based on colouring of tensors in our tensor networks to represent summation over indices. This appears to extend the capabilities of diagrammatic reasoning, with potential applications to our techniques, and semantics even outside of quantum physics.

The present paper has three sections, in Section II we introduce the elements of our graphical calculus with a particular emphasis on bipartite systems and vectorization of linear operators that are important in the subsequent sections. In Section III we introduce the mathematical representations of CP-maps listed in Fig. 1, and their corresponding graphical representation. In Section IV we describe how one may transform between any of the representations of CP-maps as shown by the arrows in Fig. 1. In this figure the type of arrow connecting two boxes depicts the type of transformation between the corresponding CP map representations. The solid arrows depict linear transformations, while the transformations depicted by dashed arrows are non-linear. Here the utility of our graphical calculus manifests as all the linear transformations correspond to wire-bending operations in our tensor diagrams, yet the corresponding algebraic expressions involve complicated manipulations. In addition, the bi-directional arrows depict invertible (bijective) transformations, while the single directional arrows depict non-invertible transformations, where either injectivity (solid arrows), or surjectivity (dashed arrow) fails.

In the present paper we will use the notation that $\mathcal{X}, \mathcal{Y}, \mathcal{Z}$ are finite-dimensional complex Hilbert spaces, $\mathcal{L}(\mathcal{X}, \mathcal{Y})$ is the space of bounded linear operators $A : \mathcal{X} \to \mathcal{Y}$ (with $\mathcal{L}(\mathcal{X}) \equiv \mathcal{L}(\mathcal{X}, \mathcal{X})$), $\mathcal{T}(\mathcal{X}, \mathcal{Y})$ is the space of operator maps $\mathcal{E} : \mathcal{L}(\mathcal{X}) \to \mathcal{L}(\mathcal{Y})$ (with $\mathcal{T}(\mathcal{X}) \equiv \mathcal{T}(\mathcal{X}, \mathcal{X})$), and $\mathcal{C}(\mathcal{X}, \mathcal{Y})$ is the space of operator maps $\mathcal{E}$ which are CPTP.

II. TENSOR NETWORKS

Tensors can bethought of as indexed multi-dimensional arrays of complex numbers with respect to a fixed standard basis. The number of indices is called the *order* of a tensor, and the concurrent evaluation of all indices returns a complex number. For example, consider the Hilbert space $\mathcal{X} \cong \mathbb{C}^d$, where as is typical in QIP, we choose our standard basis to be the *computational basis* $\{|i\rangle : i = 0, ..., d-1\}$. Then in Dirac notation a vector $|v\rangle \in \mathcal{X}$ is a 1st-order tensor which can be expressed in terms of its tenor components $v_i := \langle i|v\rangle$ with respect to the standard basis as $|v\rangle = \sum_{i=0}^{d-1} v_i |i\rangle$. Similarly one can represent linear operators on this Hilbert space, $A \in \mathcal{L}(\mathcal{X})$, as 2nd-order tensors with components $A_{ij} := \langle i|A|j\rangle$ as $A = \sum_{i,j=0}^{d-1} A_{ij} |i\rangle\langle j|$.

Hence, in Dirac notation the number of indices of a tensors components are what we refer to as the order of the tensor. Vectors $|v\rangle \in \mathcal{X}$ refer to tensors which only have *ket* "$|i\rangle$" basis elements, vectors in the dual vector space

$\langle u| \in \mathcal{X}^\dagger$ refer to those with only *bra's* "$\langle i|$", and linear operators on $A \in \mathcal{L}(\mathcal{X})$ refer to tensors with a mixture of kets and bras in their component decomposition.

The idea of representing states, operators and process (etc.) diagrammatically dates back to several works by Penrose and is often referred to as *Penrose graphical notation* or *string diagrams*. We adopt Penrose's notation of representing states (vectors) and effects (dual-vectors) as triangles, linear operators as boxes, and scalars as diamonds, as illustrated in Fig. 2. Here each index corresponds to an open wire on the diagram and so we may define higher order tensors with increasingly more wires. The number of wires is then the order of the tensor, with each wire acting on a separate vector space $\mathcal{X}_j$.

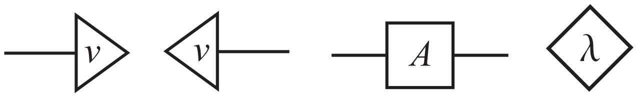

(a) Vector $|v\rangle \in \mathcal{X}$ (b) Dual-vector $\langle v| \in \mathcal{X}^\dagger$ (c) Linear Operator $A \in \mathcal{L}(\mathcal{X})$ (d) Scalar $\lambda \in \mathbb{C}$

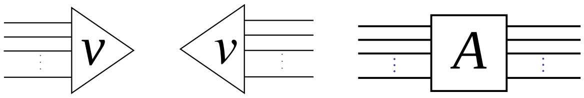

(e) Vector $|v\rangle \in \bigotimes_{i=1}^n \mathcal{X}_i$ (f) Dual-vector $\langle v| \in \bigotimes_{i=1}^n \mathcal{X}_i^\dagger$ (g) Linear operator $A : \bigotimes_{i=1}^n \mathcal{X}_i \to \bigotimes_{j=1}^m \mathcal{X}_j$

FIG. 2. Elementary tensors.

We also insist that the orientation of these wires, rather than the number of wires, specifies whether they represent multi-partite vectors, dual-vectors, or linear operators. We have a freedom in choosing our orientation for the tensors, top-to-bottom, bottom-to-top, left-to-right or right-to-left. In this paper we will choose the *right-to-left* convention (the opposite of most orthodox quantum circuits) so that the graphical representation will most closely match the underlying equations. Thus we use the terms *vector*, *dual-vector* and *linear operator* to refer to tensors of any order, not just 1st-order and 2nd-order, based on the orientation of their wires as follows:

1. *Vectors* $|v\rangle \in \bigotimes_{j=1}^n \mathcal{X}_j$ are tensors with n wires oriented to the left.

2. *Vectors in the dual space* $\langle v| \in \bigotimes_{j=1}^n \mathcal{X}_j^\dagger$ are tensors with n wires are oriented to the right.

3. *Linear operators* $A : \bigotimes_{i=1}^n \mathcal{X}_i \to \bigotimes_{j=1}^m \mathcal{X}_j$ are tensors which have n wires going to the right and m wires to the left.

4. Tensors with no open wires are *Scalars* $\lambda \in \mathbb{C}$.

The graphical depictions of the these tensors are also illustrated in Fig. 2. In the present paper, we will generally be interested in the case where each wire indexes $\mathcal{X}_j \cong \mathbb{C}^d$ for fixed dimension d, though one may generalize most of what follows to situations where the dimensions of each wire are not equal. Note that we represent scalars as tensors with no open wires, this could either be a contracted tensor $\lambda = \langle v|u\rangle$, or a multiplicative factor λ acting on the tensor A as λA.

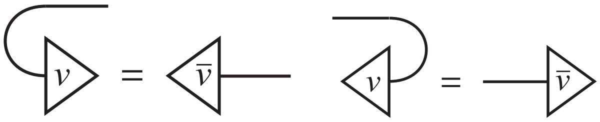

(a) Vector transposition: $|v\rangle^T = \langle \overline{v}|$ (b) Dual-vector transposition: $\langle v|^T = |\overline{v}\rangle$

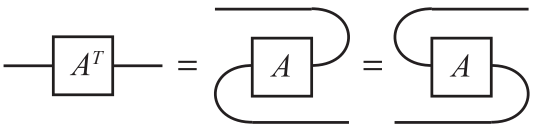

(c) Linear operator transposition

FIG. 3. Graphical depiction of transposition by wire bending.

The mathematical rules of tensor network theory assert that the wires of tensors may be manipulated, with each manipulation corresponding to a specific operation with equational meaning. We now introduce some tools which we have tailored for manipulations common in open quantum systems. Transposition of a 2nd-order tensor is represented a bending of a tensors wires as illustrated in Fig. 3. Complex conjugation of a tensor's coefficients however is depicted by a bar over the tensor label in the diagram as illustrated in Fig. 4. Hence we may represent the transformation of a vector to its dual vector, or the hermitian conjugation of a linear operator as the combination of these two operations as illustrated in Fig. 5. We stress that under this convention a vector $|v\rangle = \sum_i v^i|i\rangle$ and its hermitian conjugate dual-vector $\langle v| = \sum_i \overline{v}_i\langle i|$ are represented as shown in Fig. 2a and 2b respectively.

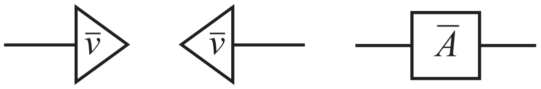

(a) Complex conjugation of vector $|v\rangle$ (b) Complex conjugation of dual vector $\langle v|$ (c) Complex conjugation of operator A

FIG. 4. Graphical depiction complex conjugation.

Tensor contraction is represented by joining the wires corresponding to the indices to be contracted. In the case of matrix multiplication $A \cdot B$ is represented by connecting the corresponding wires of the tensors representing the matrices as shown in Fig. 6a. To form multi-partite tensors we denote the tensor product of two tensors $A \otimes B$ by the vertical juxtaposition of their tensor networks as shown in Fig. 6b. The trace of an operator by depicted

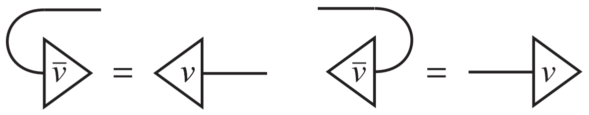

(a) Hermitian conjugation of a vector : $|v\rangle^\dagger = \langle v|$

(b) Hermitian conjugation of a dual-vector : $\langle v|^\dagger = |v\rangle$

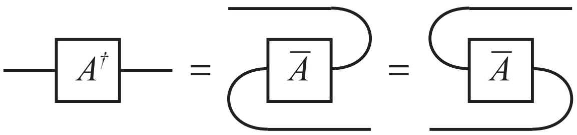

(c) Hermitian Conjugation of an operator A

FIG. 5. Graphical depiction of hermitian conjugation.

by connecting the corresponding left and right wires of a linear operator as illustrated in Fig. 7.

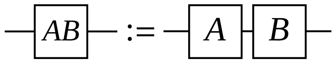

(a) Matrix multiplication

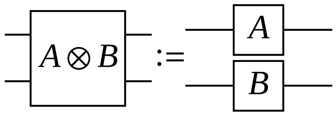

(b) Tensor product

FIG. 6. Vertical (b) and horizontal (a) Composition of tensors.

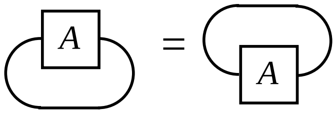

FIG. 7. Tensor network for the trace of a linear operator A.

We represent summation in our variant of graphical calculus adapted to open systems by introducing shading or colouring of the tensors being summed over (we call this the colour summation convention). Tensors corresponding to the same summation index will be shaded the same colour, and we use different colours for different summation indexes. For example, consider the spectral decomposition of a normal operator A with eigenvalues and eigenvectors λ_i and $|a_i\rangle$ respectively. The graphical spectral-decomposition $A = \sum_i \lambda_i |a_i\rangle$ using our graphical summation convention is illustrated in Fig. 8.

In our colour summation convention, we will represent the sum over the standard basis as a shaded vector (or dual-vector) tensor with an empty label. This is illustrated in the graphical resolution of the identity appearing in Fig 9.

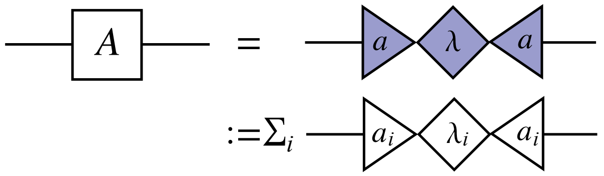

FIG. 8. Illustration of our colour summation convention using the spectral decomposition of a normal operator.

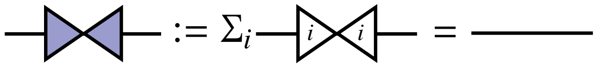

FIG. 9. Graphical resolution of the identity using the colour summation convention.

The unnormalized maximally entangled Bell-state

$$|\Phi^+\rangle = \sum_{i=0}^{d} |i\rangle \otimes |i\rangle \in \mathcal{X} \otimes \mathcal{X}, \tag{1}$$

is represented graphically as the curve shown in Fig. 10a. Similarly the Bell-effect $\langle\Phi^+|$ is represented as shown in Fig. 10b.

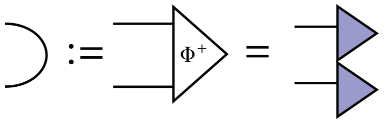

(a) Bell-state

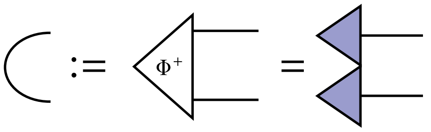

(b) Dual Bell-state or *Bell effect*

FIG. 10. The graphical depiction of the unnormalized Bell-state $|\Phi^+\rangle$ and its dual $\langle\Phi^+|$.

As will be shown in Section II B, our choice of graphical notation for $|\Phi^+\rangle$ is due to its equivalence to the vectorization of the identity operator.

Using the graphical definition for $|\Phi^+\rangle$ we can compose the bell-state and its dual to form an identity element [2]. This is known as the *snake equation* and is shown in Fig. 11.

The snake equations have several uses and provide an equivalence class of diagrams. Anytime we have a curved wire with two bends we can "pull the wire" to straighten it out into an identity. Anytime we bend a wire, transforming between say a bra and a ket, we can bend the wire to transform back again.

By combining the snake-equation with the wire-bending operation for transposition from Fig. 3c, we find that "sliding" a linear operator around a bell-state is also

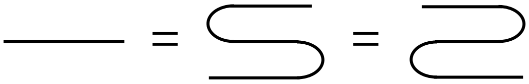

FIG. 11. The snake or zig-zag equations [2].

equivalent to transposition of the operator. This is illustrated in Fig. 12. Note that due to the orientation of the wires this graphical representation of the operator A is actually a vector. This is called the vectorization of a matrix and we discuss this in more detail in Section II B.

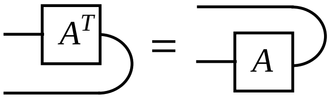

FIG. 12. Graphical depiction of transposition by "sliding" around a bell-state.

Another important operation is the graphical SWAP which exchanges the position of two Hilbert spaces in a composite system. Let $\mathcal{X}$ and $\mathcal{Y}$ be complex Hilbert spaces of dimensions d_1 and d_2 respectively, then the SWAP operation is the map

$$\mathrm{SWAP} : \mathcal{X} \otimes \mathcal{Y} \to \mathcal{Y} \otimes \mathcal{X} \tag{2}$$

$$\mathrm{SWAP} : |x\rangle \otimes |y\rangle \mapsto |y\rangle \otimes |x\rangle, \tag{3}$$

for all $|x\rangle \in \mathcal{X}, |y\rangle \in \mathcal{Y}$.

Given any two orthonormal basis $\{|x_i\rangle : i = 0, \ldots, d_1 - 1\}$ and $\{|y_j\rangle : j = 0, \ldots, d_2 - 1\}$ for $\mathcal{X}$ and $\mathcal{Y}$ respectively, we can give an explicit construction for the SWAP operation as

$$\mathrm{SWAP} = \sum_{i_1=0}^{d_1-1} \sum_{j_2=0}^{d_2-1} |y_j\rangle\langle x_i| \otimes |x_i\rangle\langle y_j|. \tag{4}$$

The SWAP operation is represented graphically by two crossing wires as shown in Fig. 13. The basis decomposition in Eqn (4) is then an application of the resolution of the identity from Fig. 9 to each wire. In Section II B we will see that the SWAP operation is the natural transformation between the row-stacking and column-stacking vectorization conventions.

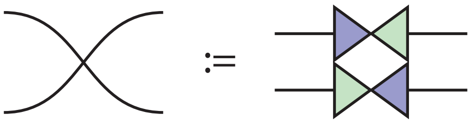

FIG. 13. The SWAP operation in our graphical calculus (left) and it's decomposition in terms of the standard basis using our colour summation convention (right).

A. Bipartite Matrix Operations

Bipartite matrices are used in several representations of CP-maps, and manipulations of these matrices will be important in the following discussion. Consider two complex Hilbert spaces $\mathcal{X}$, and $\mathcal{Y}$ with dimensions d_x and d_y respectively. The bipartite matrices we are interested in are then $d_x^2 \times d_y^2$ matrices $M \in \mathcal{L}(\mathcal{X} \otimes \mathcal{Y})$ which we can represent as 4th-order tensors with tensor components

$$M_{m\mu,n\nu} := \langle m, \mu | M | n, \nu \rangle \tag{5}$$

where $m, n \in \{0, ..., d_x - 1\}$, $\mu, \nu \in \{0, ..., d_y - 1\}$ and $|n, \nu\rangle := |n\rangle \otimes |\nu\rangle \in \mathcal{X} \otimes \mathcal{Y}$ is the tensor product of the standard bases for $\mathcal{X}$ and $\mathcal{Y}$.

We can also express the matrix M as a 2nd-order tensor in terms of the standard basis $\{|\alpha\rangle : \alpha = 0, \ldots, D-1\}$ for $\mathcal{X} \otimes \mathcal{Y}$ where $D = d_x d_y$. In this case M has tensor components

$$M_{\alpha\beta} = \langle \alpha | M | \beta \rangle \tag{6}$$

This is represented graphically in Fig. 14. We can specify the equivalence between the tensor components $M_{\alpha\beta}$ and $M_{m\mu,n\nu}$ by making the assignment

$$\alpha = d_y m + \mu \tag{7}$$

$$\beta = d_y n + \nu, \tag{8}$$

where d_y is the dimension of the Hilbert space $\mathcal{Y}$.

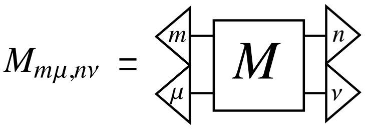

(a) 4th-order tensor components of a bipartite matrix M

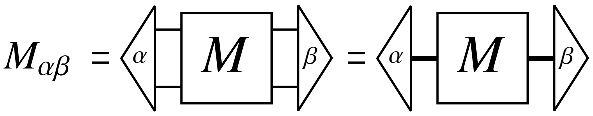

(b) 2nd-order tensor components of a bipartite matrix M

FIG. 14. Tensor components of a Bipartite matrix $M \in \mathcal{L}(\mathcal{X} \otimes \mathcal{X})$.

The bipartite matrix operations which are the most relevant for open quantum systems (see Fig. 1) are the *partial trace over* $\mathcal{X}$ ($\mathrm{Tr}_{\mathcal{X}}$) (and $\mathrm{Tr}_{\mathcal{Y}}$ over $\mathcal{Y}$), *transposition* (T), *bipartite-SWAP* (S), *col-reshuffling* (R_c), and *row-reshuffling* (R_r). The corresponding graphical manipulations are in Fig. 15 and in terms of the tensor components of M, these operations are respectively given by:

$$\begin{aligned}
\mathrm{Tr}_{\mathcal{X}} : \mathcal{L}(\mathcal{X}\otimes\mathcal{Y}) &\longrightarrow \mathcal{L}(\mathcal{Y})\\
M_{m\mu,n\nu} &\longmapsto \sum_m M_{m\mu,m\nu}\\
\mathrm{Tr}_{\mathcal{Y}} : \mathcal{L}(\mathcal{X}\otimes\mathcal{Y}) &\longrightarrow \mathcal{L}(\mathcal{X})\\
M_{m\mu,n\nu} &\longmapsto \sum_\mu M_{m\mu,n\mu}\\
T : \mathcal{L}(\mathcal{X}\otimes\mathcal{Y}) &\longrightarrow \mathcal{L}(\mathcal{X}\otimes\mathcal{Y})\\
M_{m\mu,n\nu} &\longmapsto M_{n\nu,m\mu}\\
S : \mathcal{L}(\mathcal{X}\otimes\mathcal{Y}) &\longrightarrow \mathcal{L}(\mathcal{Y}\otimes\mathcal{X})\\
M_{m\mu,n\nu} &\longmapsto M_{\mu m,\nu n}\\
R_c : \mathcal{L}(\mathcal{X}\otimes\mathcal{Y}) &\longrightarrow \mathcal{L}(\mathcal{X}\otimes\mathcal{X},\mathcal{Y}\otimes\mathcal{Y})\\
M_{m\mu,n\nu} &\longmapsto M_{mn,\mu\nu}\\
R_r : \mathcal{L}(\mathcal{X}\otimes\mathcal{Y}) &\longrightarrow \mathcal{L}(\mathcal{Y}\otimes\mathcal{Y},\mathcal{X}\otimes\mathcal{X})\\
M_{m\mu,n\nu} &\longmapsto M_{\nu\mu,nm}
\end{aligned}$$

Note that we will generally use reshuffling R to refer to col-reshuffling R_c.

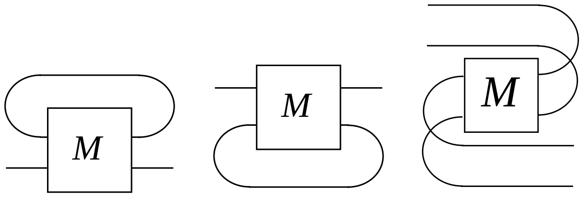

(a) Partial Trace $\mathrm{Tr}_{\mathcal{X}}(M)$ (b) Partial Trace $\mathrm{Tr}_{\mathcal{Y}}(M)$ (c) Transpose M^T

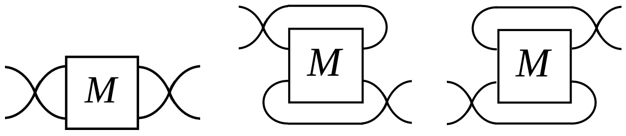

(d) Bipartite-Swap M^S (e) Row-reshuffle M^{R_r} (f) Col-reshuffle M^{R_c}

FIG. 15. Tensor networks for common Bipartite matrix manipulations.

B. Vectorization of Matrices

We now recall the concept of *vectorization* which is a reshaping operation, transforming a $(m\times n)$-matrix into a $(1\times mn)$-vector [15]. This is necessary for the description of open quantum systems in the superoperator formalism, which we will consider in Section III C. Vectorization can be done with using one of two conventions: *column-stacking* (col-vec) or *row-stacking* (row-vec). Consider two complex Hilbert spaces $\mathcal{X}\cong\mathbb{C}^m, \mathcal{Y}\cong\mathbb{C}^n$, and linear operators $A\in\mathcal{L}(\mathcal{X},\mathcal{Y})$ from $\mathcal{X}$ to $\mathcal{Y}$. Vectorization is one of two mappings

$$\text{row-vec: } \mathcal{L}(\mathcal{X},\mathcal{Y})\to\mathcal{Y}\otimes\mathcal{X} :\ A\mapsto |A\rangle\rangle_r \tag{9}$$

$$\text{col-vec: } \mathcal{L}(\mathcal{X},\mathcal{Y})\to\mathcal{X}\otimes\mathcal{Y} :\ A\mapsto |A\rangle\rangle_c \tag{10}$$

where the operation col(row)-vec when applied to a matrix, outputs a vector with the columns (rows) of the matrix stacked on top of each other. Graphical representations for the row-vec and col-vec operations are found from bending a wire to the left either clockwise or counterclockwise respectively. This is illustrated in Fig. 16.

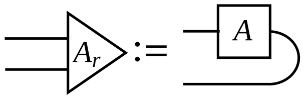

(a) Row-vec

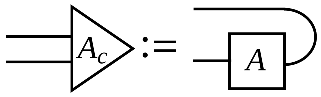

(b) Col-vec

FIG. 16. Tensor networks for Vectorization in the (a) row and (b) column conventions are found from a wire bending duality.

Vectorized matrices in the col-vec and row-vec conventions are naturally equivalent under wire exchange (the SWAP operation) as illustrated in Fig. 17.

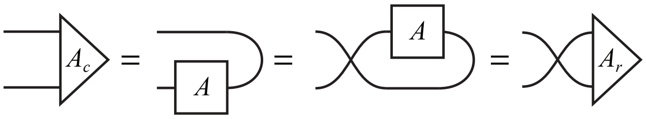

FIG. 17. Col-vec and row-vec vectorized matrices are naturally equivalent under the SWAP operation.

We may also define a vectorization operation with respect to an arbitrary basis for $\mathcal{L}(\mathcal{X},\mathcal{Y})$. Let $\mathcal{X}\cong\mathbb{C}_{d_x}, \mathcal{Y}\cong\mathbb{C}^{d_y}$, and $D=d_xd_y$. Vectorization with respect to an orthonormal operator basis $\{\sigma_\alpha : \alpha=0,...,D-1\}$ for $\mathcal{L}(\mathcal{X},\mathcal{Y})$ is given by

$$\sigma\text{-vec: } \mathcal{L}(\mathcal{X})\to\mathcal{X}\otimes\mathcal{X} :\ A\mapsto |A\rangle\rangle_\sigma. \tag{11}$$

This operation extracts the coefficients of the basis elements returning the vector

$$|A\rangle\rangle_\sigma := \sum_{\alpha=0}^{D-1}\mathrm{Tr}[\sigma_\alpha^\dagger A]|\alpha\rangle \tag{12}$$

where $\{|\alpha\rangle : \alpha=0,...,D-1\}$ is the standard basis for $\mathcal{X}\otimes\mathcal{Y}$. This is depicted in our graphical calculus in Fig. 18.

To distinguish between these different conventions use the notation $|A\rangle\rangle_x$ to denote the vectorization of a matrix

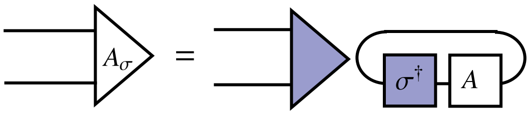

FIG. 18. Tensor network for σ-vectorization (12) with respect to an orthonormal operator basis $\{\sigma_\alpha\}$.

A, were the subscript $x = c, r, \sigma$ labels which convention we use; either c for col-vec, r for row-vec, or σ for an arbitrary basis.

For the case $\mathcal{X} \cong \mathcal{Y} \cong \mathbb{C}^d$, we can define row-vec and col-vec in terms terms of Eqn (12) by taking our basis to be the elementary matrix basis $\{E_{i,j} = |i\rangle\langle j| : i, j = 0, ..., d^2 - 1\}$ and making the assignment $\alpha = di + j$ and $\alpha = i + dj$ respectively. Hence we have

$$|A\rangle\rangle_r := \sum_{i,j=0}^{d-1} A_{ij}\, |i\rangle \otimes |j\rangle \tag{13}$$

$$|A\rangle\rangle_c := \sum_{i,j=0}^{d-1} A_{ij}\, |j\rangle \otimes |i\rangle \tag{14}$$

for row-vec (13) and col-vec (14). From the definition of the Bell state $|\Phi^+\rangle$ and summing over i and j in Equations (13) and (14) respectively one can rewrite this as

$$|A\rangle\rangle_r = (A \otimes \mathbb{1})|\Phi^+\rangle \tag{15}$$

$$|A\rangle\rangle_c = (\mathbb{1} \otimes A)|\Phi^+\rangle \tag{16}$$

which are the equational versions of Fig.s 16a and 16b respectively.

When working in the superoperator formalism for open quantum systems, it is sometimes convenient to transform between vectorization conventions in different bases. Given two orthonormal operator bases $\{\sigma_\alpha\}$ and $\{\omega_\alpha\}$ for $\mathcal{L}(\mathcal{X}, \mathcal{Y})$, the basis transformation operator

$$T_{\sigma\to\omega} : \mathcal{X} \otimes \mathcal{Y} \to \mathcal{X} \otimes \mathcal{Y} : |A\rangle\rangle_\sigma \mapsto |A\rangle\rangle_\omega \tag{17}$$

transforms vectorized operators in the σ-vec convention to the ω-vec convention as illustrated in Fig. 19.

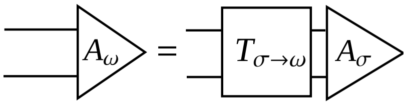

FIG. 19. Tensor network for the change of vectorization basis for a vectorized operator A from the σ-vec convention to the ω-vec convention.

The basis transformation operator $T_{\sigma\to\omega}$ is given by the equivalent expressions

$$T_{\sigma\to\omega} = \sum_\alpha |\alpha\rangle\langle\langle\omega_\alpha|_\sigma \tag{18}$$

$$= \sum_\alpha |\sigma_\alpha\rangle\rangle_\omega \langle\alpha|, \tag{19}$$

and the corresponding tensor networks are given in Fig. 20. The proof's of Eqn (18,19) are found in Appendix B.

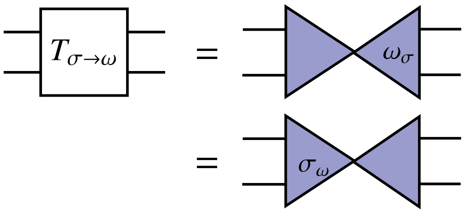

FIG. 20. Tensor networks for the change of vectorization basis operator $T_{\sigma\to\omega}$ from the σ-vec to ω-vec conventions, where $\{\sigma_\alpha\}, \{\omega_\alpha\}$ are orthonormal bases for $\mathcal{L}(\mathcal{X}, \mathcal{Y})$.

For the remainder of this paper we will use the col-vec convention by default, and drop the vectorization label subscripts unless referring to a general σ-basis. The main transformation we will be interested in is then from col-vec to another arbitrary orthononormal operator basis $\{\sigma_\alpha\}$. Tensor networks for the change of basis $T_{c\to\sigma}$ and its inverse $T_{\sigma\to c}$ are respectively illustrated in Fig. 21.

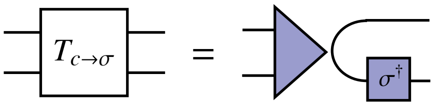

(a) Col-vec to σ-basis

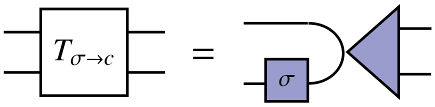

(b) σ-basis to col-vec

FIG. 21. Vectorization change of basis operators between col-vec convention and an orthonormal basis $\{\sigma_\alpha\}$ for $\mathcal{L}(\mathcal{X}, \mathcal{Y})$.

As was illustrated in Fig. 17, in the case where the second basis is the row-vec convention we have

$$T_{c\to r} = T_{r\to c} = \text{SWAP}. \tag{20}$$

One final important result that often arises when dealing with vectorized matrices is Roth's Lemma for the vectorization of the matrix product ABC [15]. Given matrices $A, B, C \in \mathcal{L}(\mathcal{X})$ we have

$$|ABC\rangle\rangle = (C^T \otimes A)|B\rangle\rangle \tag{21}$$

The graphical tensor network proof of this lemma is found in Fig. 22.

III. REPRESENTATIONS OF COMPLETELY POSITIVE MAPS

Before presenting the main results found in this study we first recall several common mathematical descriptions

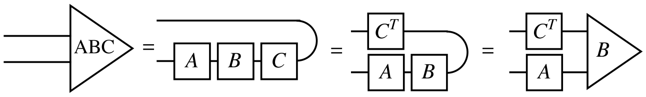

FIG. 22. Graphical proof of Roth's lemma (21) in col-vec convention.

for completely-positive trace-preserving maps, and show how several key properties may be captured graphically using the diagrammatic notation we have developed specific for this purpose. The representations we will consider are the Kraus (or operator-sum) representation, the system-environment (or Stinespring) representation, the Liouville superoperator description based on vectorization of matrices, and the Choi-matrix or dynamical matrix description based on the Choi-Jamiołkowski isomorphism. We will also describe the often used process matrix representation and show how this can be considered as a change of basis of the Choi-matrix. Following this, in Section IV we will show how our framework now enables one to freely transform between these representations as illustrated in Fig. 1.

A. Kraus / Operator-Sum Representation

The first representation of CPTP-maps we cast into our framework is the *Kraus* [16] or *operator-sum* [1] representation. This representation is particularly useful in phenomenological models of noise in quantum systems. Kraus's theorem states that a linear map $\mathcal{E} \in \mathcal{T}(\mathcal{X}, \mathcal{Y})$ is CPTP if and only if it may be written in the form

$$\mathcal{E}(\rho) = \sum_{\alpha=0}^{D} K_\alpha \rho K_\alpha^\dagger \tag{22}$$

where the Kraus operators $\{K_\alpha : \alpha = 0, ..., D-1\}$, $K_\alpha \in \mathcal{L}(\mathcal{X}, \mathcal{Y})$, satisfy the completeness relation

$$\sum_{\alpha=0}^{D} K_\alpha^\dagger K_\alpha = \mathbb{1}_\mathcal{X}. \tag{23}$$

This Kraus evolution has the graphical representation shown in Fig. 23.

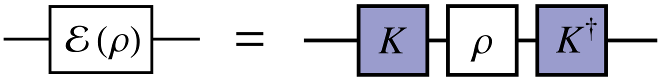

FIG. 23. Tensor network for the evolution of a state ρ under a CP-map $\mathcal{E}$ in the Kraus representation (22).

The maximum number of Kraus operators needed for a Kraus description of $\mathcal{E}$ is equal to the dimension of $\mathcal{L}(\mathcal{X}, \mathcal{Y})$. For the case where $\mathcal{X} \cong \mathcal{Y} \cong \mathbb{C}^d$ the maximum number of Kraus operators is d^2, and the minimum number case corresponds to unitary evolution where there is only a single Kraus operator.

It is important to note that the Kraus representation of $\mathcal{E}$ is not unique as there is unitary freedom in choosing the Kraus operators. We can give preference to a particular representation called the *Canonical Kraus Representation* [17] which is the unique set of Kraus operators satisfying the orthogonality relation $\mathrm{Tr}[K_\alpha^\dagger K_\beta] = \lambda_\alpha \delta_{\alpha\beta}$. The canonical Kraus representation will be important when transforming between representations in Section IV.

B. System-Environment / Stinespring Representation

The second representation of CPTP-maps we consider is the system-environment model [1], which is typically considered the most physically intuitive description of open system evolution. This representation is closely related to (and sometimes referred to as) the Stinespring representation as it can be thought of as an application of the Stinespring dilation theorem [18], which we also describe in this section. In this model, we consider a system of interest $\mathcal{X}$, called the *principle system*, coupled to an additional system $\mathcal{Z}$ called the *environment*. The composite system of the principle system and environment is then treated as a closed quantum system which evolves unitarily. We recover the reduced dynamics on the principle system by performing a partial trace over the environment. Suppose the initial state of our composite system is given by $\rho \otimes \tau \in \mathcal{L}(\mathcal{X} \otimes \mathcal{Z})$, where $\tau \in \mathcal{L}(\mathcal{Z})$ is the initial state of the environment. The joint evolution is described by a unitary operator $U \in \mathcal{L}(\mathcal{X} \otimes \mathcal{Z})$ and the reduced evolution of the principle system's state ρ is given by

$$\mathcal{E}(\rho) = \mathrm{Tr}_\mathcal{Z}[U(\rho \otimes \tau)U^\dagger] \tag{24}$$

For convenience we can assume that the environment starts in a pure state $\tau = |v_0\rangle\langle v_0|$, and in practice one only need consider the case where the Hilbert space describing the environment has at most dimension d^2 for $\mathcal{X} \cong \mathbb{C}^d$ [1]. The system-environment representation of the CP-map $\mathcal{E}$ may then be represented graphically as shown in Fig. 24.

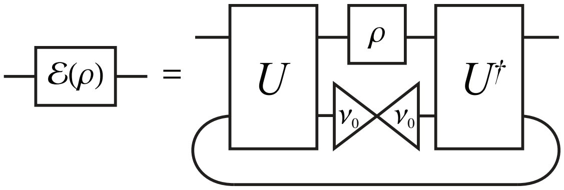

FIG. 24. Tensor network for the evolution of a state ρ by a CP-map $\mathcal{E}$ in the system-environment representation (24). The environment is initially in the state $|v_0\rangle$ and the joint evolution is given by a unitary operator U.

The system-environment model is advantageous when modelling the environment as a physical system. However, care must be taken when ascribing physical reality to any particular model as the system-environment description is not unique. This is not surprising as many different physical interactions could give rise to the same reduced dynamics on the principle system. This freedom manifests in an ability to choose the initial state of the environment in the representation and then adjust the unitary operator accordingly. In practice, the system-environment model can be cumbersome for performing many calculations where the explicit dynamics of the environment system are irrelevant. The remaining descriptions, which we cast into diagrammatic form, may be more convenient in these contexts.

Note that the system-environment evolution for the most general case will be an isometry and this is captured in Stinespring's representation [18]. Stinespring's dilation theorem states that a CP-map $\mathcal{E} \in \mathcal{C}(\mathcal{X},\mathcal{Y})$ can be written in the form

$$\mathcal{E}(\rho) = \mathrm{Tr}_Z\left[A\rho A^\dagger\right] \tag{25}$$

where $A \in \mathcal{L}(\mathcal{X},\mathcal{Y}\otimes\mathcal{Z})$ and the Hilbert space $\mathcal{Z}$ has dimension at most equal to $\mathcal{L}(\mathcal{X},\mathcal{Y})$. Further, the map $\mathcal{E}$ is trace preserving if and only if $A^\dagger A = \mathbb{1}_\mathcal{X}$ [18].

In the case where $\mathcal{Y} \cong \mathcal{X}$, the Hilbert space $\mathcal{X}\otimes\mathcal{Z}$ mapped into by the Stinespring operator A is equivalent to the joint system-environment space in the system-environment representation. Hence, as illustrated in Fig. 25, one may move from the system-environment description to the Stinespring representation by letting

$$A = U\cdot(\mathbb{1}_\mathcal{X}\otimes|v_0\rangle), \tag{26}$$

where $|v_0\rangle \in \mathcal{Z}$ is the initial state of the environment.

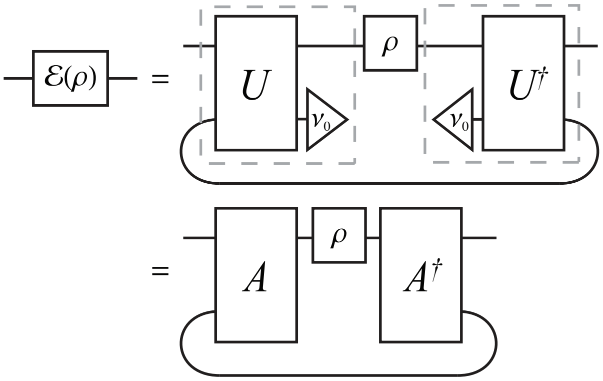

FIG. 25. Graphical depiction of the relationship between the Stinespring (25) and system-environment (24) representations of a CP map $\mathcal{E}$.

This close relationship is why these two representations are often referred to by the same name, and as we will show in Section IV E, it is however straight forward to construct a Stinespring representation from the Kraus representation. However, generating a full description of the joint system-environment unitary operator U form a Stinespring operator A is cumbersome. It involves an algorithmic completion of the matrix elements in the unitary U not contained within the subspace of the initial state of the environment [17]. Since it usually suffices to define the action of U when restricted to the initial state of the environment, which by Eqn (26) is the Stinepsring representation, this is often the only transformation one need consider.

A further important point is that the evolution of the principle system $\mathcal{E}(\rho)$ is guaranteed to be CP if and only if the initial state of the system and environment is separable; $\rho_{\mathcal{X}\mathcal{Z}} = \rho_\mathcal{X}\otimes\rho_Z$. In the case where the physical system is initially correlated with the environment, it is possible to have reduced dynamics which are non-completely positive [19–21], however such situations are beyond the scope of this paper.

C. Louiville-Superoperator Representation

We now move to the *linear superoperator* or *Liouville* representation of a CP-map $\mathcal{E} \in \mathcal{C}(\mathcal{X},\mathcal{Y})$. This representation is based on the vectorization of the density matrix $\rho \mapsto |\rho\rangle\rangle_\sigma$ with respect to some orthonormal operator basis $\{\sigma_\alpha : \alpha = 0,...,d^2-1\}$ introduced in Section II B. Once we have chosen a vectorization basis (col-vec in our case) we define the superoperator for a map $\mathcal{E} \in \mathcal{T}(\mathcal{X},\mathcal{Y})$ to be the linear map

$$\mathcal{S} : \mathcal{X}\otimes\mathcal{X} \to \mathcal{Y}\otimes\mathcal{Y} : |\rho\rangle\rangle \mapsto |\mathcal{E}(\rho)\rangle\rangle \tag{27}$$

This is illustrated in Fig. 26.

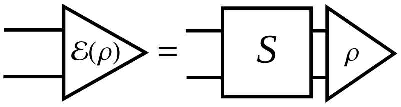

FIG. 26. Tensor network for the evolution of a state ρ by CP-map $\mathcal{E}$ in the superoperator representation (27).

In the col-vec basis we can express the evolution of a state ρ in terms of tensor components of $\mathcal{S}$ as

$$\mathcal{E}(\rho)_{mn} = \sum_{\mu\nu}\mathcal{S}_{nm,\nu\mu}\rho_{\mu\nu}. \tag{28}$$

For the case where $\mathcal{E} \in \mathcal{T}(\mathcal{X})$, it is sometimes useful to change the basis of our superoperators from the col-vec basis to an orthonormal operator basis $\{\sigma_\alpha\}$ for $\mathcal{L}(\mathcal{X})$. This is done using the basis transformation operator $T_{c\to\sigma}$ introduced in Section II B. We have

$$\mathcal{S}_\sigma = T_{c\to\sigma}\cdot\mathcal{S}\cdot T^\dagger_{c\to\sigma} \tag{29}$$

$$= \sum_{\alpha\beta}\mathcal{S}_{\alpha\beta}\,|\sigma_\alpha\rangle\rangle\langle\langle\sigma_\beta|. \tag{30}$$

where the subscript σ indicates that $\mathcal{S}_\sigma$ is the superoperator in the σ-vec convention. The tensor networks for this transformation is given in Fig. 27. Note that for a general map $\mathcal{E} \in \mathcal{T}(\mathcal{X},\mathcal{Y})$ we could do a similar construction but would need different bases for the initial and final Hilbert spaces $\mathcal{L}(\mathcal{X})$ and $\mathcal{L}(\mathcal{Y})$.

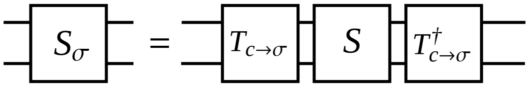

FIG. 27. Tensor network for changing vectorization convention of a superoperator from col-vec to an arbitrary operator basis $\{\sigma_\alpha\}$.

The structural properties the superoperator $\mathcal{S}$ must satisfy for the linear map $\mathcal{E}$ to be trace-preserving (TP), hermitian-preserving (HP) and completely positive (CP) are [17]:

$$\mathcal{E} \text{ is HP} \iff \overline{\mathcal{S}} = \mathcal{S}^S \tag{31}$$

$$\iff \tag{32}$$

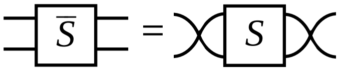

$$\mathcal{E} \text{ is TP} \iff \mathcal{S}_{mm,n\nu} = \delta_{n\nu} \tag{33}$$

$$\iff \tag{34}$$

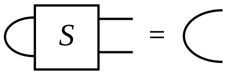

$$\mathcal{E} \text{ is CP} \iff \mathcal{S}_{\mathcal{I}\otimes\mathcal{E}}|\rho_{AB}\rangle\rangle \geq 0 \;\forall \rho_{AB} \geq 0 \tag{35}$$

Note that there is not a convenient structural criteria on the superoperator $\mathcal{S}$ which specifies if $\mathcal{E}$ is a CP-map to test for positivity or complete positivity one generally uses the closely related *Choi Matrix* representation.

Superoperators are convenient to use for many practical calculations. Unlike the system-environment model the superoperator S is unique with respect to our choice of vectorization basis. Choosing an appropriate basis to express the superoperator in can often expose certain information about a quantum system. For example, if we want to model correlated noise for a mutli-partite system we can vectorize with respect to the mutli-qubit Pauli basis. Correlated noise would then manifest as non-zero entries in the superoperator corresponding to terms such as $\sigma_x\otimes\sigma_x$. One can perform this transformation by using the tensor network shown in Fig. 27.

D. Choi-Matrix Representation

The final representation shown in Fig. 1 is the *Choi matrix* [22], or dynamical matrix [17]. This is an application of the Choi-Jamiołkowski isomorphism which gives a bijection between linear maps and linear operators [23]. Similarly to how vectorization mapped linear operators in $\mathcal{L}(\mathcal{X},\mathcal{Y})$ to vectors in $\mathcal{X}\otimes\mathcal{Y}$ or $\mathcal{Y}\otimes\mathcal{X}$, the Choi-Jamiołkowski isomorphism maps linear operators in $\mathcal{T}(\mathcal{X},\mathcal{Y})$ to linear operators in $\mathcal{L}(\mathcal{X}\otimes\mathcal{Y})$ or $\mathcal{L}(\mathcal{Y}\otimes\mathcal{X})$. The two conventions are

$$\text{col-}\Lambda : \mathcal{T}(\mathcal{X},\mathcal{Y}) \to \mathcal{L}(\mathcal{X}\otimes\mathcal{Y}) : \;\mathcal{E} \mapsto \Lambda_c \tag{36}$$

$$\text{row-}\Lambda : \mathcal{T}(\mathcal{X},\mathcal{Y}) \to \mathcal{L}(\mathcal{Y}\otimes\mathcal{X}) : \;\mathcal{E} \mapsto \Lambda_r. \tag{37}$$

For $\mathcal{X} \cong \mathbb{C}^d$, the explicit construction of the Choi-matrix is given by

$$\Lambda_c = \sum_{i,j=0}^{d-1} |i\rangle\langle j| \otimes \mathcal{E}(|i\rangle\langle j|) \tag{38}$$

$$\Lambda_r = \sum_{i,j=0}^{d-1} \mathcal{E}(|i\rangle\langle j|) \otimes |i\rangle\langle j| \tag{39}$$

where $\{|i\rangle : i = 0,\ldots,d-1\}$ is an orthonormal basis for $\mathcal{X}$.

We call the two conventions col-Λ and row-Λ due to their relationship with the vectorization conventions introduced in Section II B. The Choi-Jamiołkowski isomorphism can also be thought of as having a map $\mathcal{E} \in \mathcal{T}(\mathcal{X},\mathcal{Y})$ act on one half of a Bell state $|\Phi^+\rangle = \sum_i |i\rangle \otimes |i\rangle \in \mathcal{L}(\mathcal{X}\otimes\mathcal{X})$, and hence these conventions corresponding to which half of the Bell state it acts on:

$$\Lambda_c = (\mathcal{I}\otimes\mathcal{E})|\Phi^+\rangle\langle\Phi^+| \tag{40}$$

$$\Lambda_r = (\mathcal{E}\otimes\mathcal{I})|\Phi^+\rangle\langle\Phi^+| \tag{41}$$

where $\mathcal{I} \in \mathcal{T}(\mathcal{X},\mathcal{X})$ is the identity map. In what follows we will use the col-Λ convention and drop the subscript from Λ_c. We note that the alternative row-Λ Choi-matrix is naturally obtained by applying the bipartite-SWAP operation to Λ_c.

As will be considered in Section IV C, if the evolution of the CP map $\mathcal{E}$ is described by a Kraus representation $\{K_i\}$, then the Choi-Jamiołkowski isomorphism states that we construct the Choi-matrix by acting on one half of a bell state with the Kraus map. This is illustrated in Fig. 28.

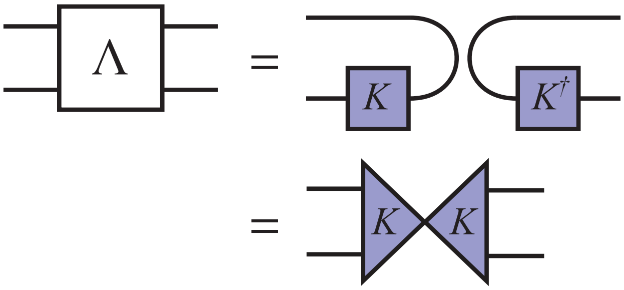

FIG. 28. A graphical depiction of the Choi-Jamiołkowski isomorphism for a Kraus description of a CP map $\mathcal{E}$. Note that in general any tensor network describing a linear map $\mathcal{E}$, not just the Kraus description, may be contracted with one-half of the maximally entangled state $|\Phi^+\rangle\langle\Phi^+|$ to construct the Choi-matrix.

With the Choi-Jamiołkowski isomorphism defined, the evolution of a quantum state in terms of the Choi-matrix is then given by

$$\mathcal{E}(\rho) = \mathrm{Tr}_{\mathcal{X}}\left[(\rho^T \otimes \mathbb{1}_{\mathcal{Y}})\Lambda\right] \tag{42}$$

or in terms of tensor components

$$\mathcal{E}(\rho)_{mn} = \sum_{n,m} \Lambda_{\mu m,\nu n}\rho_{\mu\nu}. \tag{43}$$

The tensor network for Eqn (42) is given in Fig. 29, and the graphical proof for the case where $\mathcal{E}$ is described by a Kraus representation is given in Fig. 30.

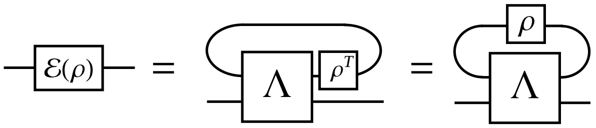

FIG. 29. Tensor network for the evolution of a state ρ by CP-map $\mathcal{E}$ in the Choi-matrix representation (42).

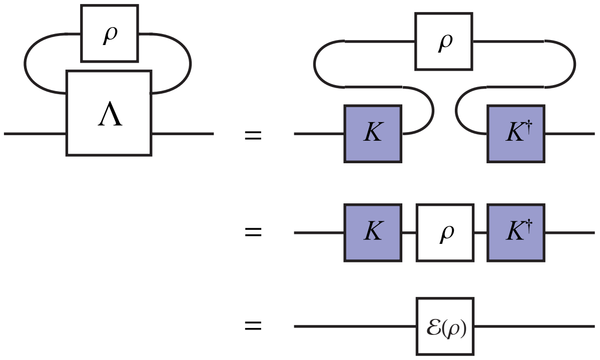

FIG. 30. Proof of (42) assuming a Kraus representation of a CP-map $\mathcal{E}$ (Fig. 23) and using the snake-equations (Fig. 11).

The structural properties the Choi-matrix Λ must satisfy for the linear map $\mathcal{E}$ to be trace-preserving (TP), hermitian-preserving (HP) and completely positive (CP) are [17]:

$$\mathcal{E} \text{ is HP} \iff \Lambda^\dagger = \Lambda \tag{44}$$

$\iff$
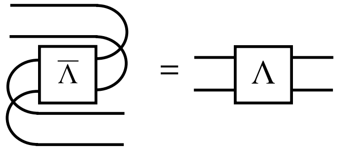

(45)

$$\mathcal{E} \text{ is TP} \iff \mathrm{Tr}_{\mathcal{Y}}[\Lambda] = \mathbb{1}_{\mathcal{X}} \tag{46}$$

$\iff$
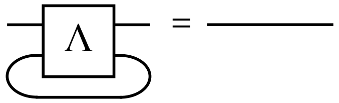

(47)

$$\mathcal{E} \text{ is CP} \iff \mathcal{E} \text{ is CP} \iff \Lambda \geq 0. \tag{48}$$

The Choi-matrix for a given map $\mathcal{E}$ is unique with respect to the isomorphism convention chosen. We will provide tensor networks to illustrate a close relationship to the superoperator formed with the corresponding vectorization convention in Section IV A. The Choi-matrix finds practical utility as one can check the complete-positivity of the map $\mathcal{E}$ by computing the eigenvalues of Λ, and it is also necessary to construct the Choi-matrix for a given superoperator to transform to the other representations.

Due to the similarity of vectorization and the Choi-Jamiołkowski isomorphism, one could then ask what happens if we vectorize in a different basis. This change of basis of the Choi-matrix is more commonly known as the χ-matrix which we will discuss next. However, such a change of basis does not change the eigen-spectrum of a matrix, so the positivity criteria in Eqn (48) holds for any basis.

Another desirable property of Choi matrices is that they can be directly determined for a given system experimentally by *ancilla assisted process tomography (AAPT)* [24, 25]. This is an experimental realization of the Choi-Jamiołkowski isomorphism where one prepares the maximally entangled state $\frac{1}{\sqrt{d}}\sum_{i=0}^{d}|i\rangle\otimes|i\rangle$ on the joint ancilla-system and subjects one half to the channel $\mathcal{E}$. State tomography is then performed on the output and the reconstructed state is equal to the Choi matrix up to the normalization factor d.

E. Process Matrix Representation

As previously mentioned, one could consider a change of basis of the Choi-matrix analogous to that for the superoperator. The resulting operator is more commonly known as the *χ-matrix* or *process matrix* [1]. Consider Hilbert spaces $\mathcal{X} \cong \mathbb{C}^{d_x}$, $\mathcal{Y} \cong \mathbb{C}^{d_y}$ and let $D = d_x d_y$. If one chooses an orthonormal operator basis $\{\sigma_\alpha : \alpha = 0, ..., D-1\}$ for $\mathcal{L}(\mathcal{X},\mathcal{Y})$, then a CPTP map $\mathcal{E} \in \mathcal{C}(\mathcal{X},\mathcal{Y})$ may be expressed in terms of a matrix $\chi \in \mathcal{L}(\mathcal{X}\otimes\mathcal{Y})$ as

$$\mathcal{E}(\rho) = \sum_{\alpha,\beta=0}^{D-1} \chi_{\alpha\beta}\sigma_\alpha\rho\sigma_\beta^\dagger \tag{49}$$

where the process matrix χ is unique with respect to the choice of basis $\{\sigma_\alpha\}$.

In terms of the Choi-matrix, we have that the process matrix with respect to an orthonormal operator basis $\{\sigma_\alpha\}$ is given by

$$\chi = T_{c\to\sigma}^\dagger \cdot \Lambda \cdot T_{c\to\sigma} \tag{50}$$

$$= \sum_{\alpha,\beta} \Lambda_{\alpha\beta}|\omega_\alpha\rangle\rangle\langle\langle\omega_\beta| \tag{51}$$

where $T_{c\to\sigma}$ is the vectorization change of basis operator introduced in Section II B. Thus evolution in terms of the χ-matrix is analogous to our Choi evolution as given in Fig. 31.

The graphical proof asserting the validity of Eqn (50) is given in Fig. 32. We also see that if one forms the process matrix with respect to the col-vec basis $\sigma_\alpha = E_{j,i}$ where $\alpha = i + dj$ and d is the dimension of $\mathcal{H}$, then $\chi^c = \Lambda$.

Since the process matrix is a unitary transformation of the Choi-matrix, it shares the same structural conditions for hermitian preservation and complete-positivity as for the Choi-matrix given in Eqns (44) and (48) respectively. The condition for it to be trace preserving is different

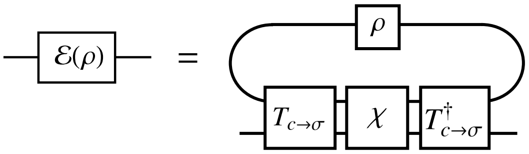

FIG. 31. Tensor network for the evolution of a state ρ by CP-map $\mathcal{E}$ in the χ-matrix representation (49). It is analogous to evolution in the Choi-matrix representation (Fig. 29).

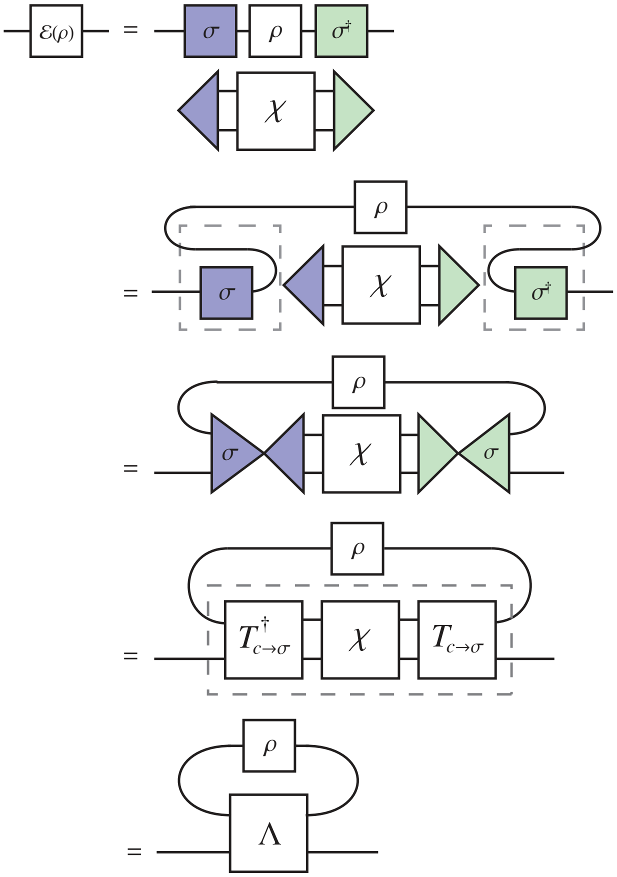

FIG. 32. Graphical proof of the equivalence of the Choi-matrix and process matrix under change of basis given in (50).

however. These conditions are

$$\mathcal{E} \text{ is TP} \iff \mathrm{Tr}_{\mathcal{Y}}\left[T_{c\to\sigma}\chi T^\dagger_{c\to\sigma}\right] = \mathbb{1}_{\mathcal{X}} \tag{52}$$

$$\mathcal{E} \text{ is HP} \iff \chi^\dagger = \chi \tag{53}$$

$$\mathcal{E} \text{ is CP} \iff \chi \geq 0. \tag{54}$$

To convert a process-matrix χ in a basis $\{\sigma_\alpha\}$ to another orthonormal operator basis $\{\omega_\alpha\}$, we may use the inverse transformation to the superoperator change of basis from Section III C. That is

$$\chi^\omega = T^\dagger_{\sigma\to\omega}\cdot\chi^\sigma\cdot T_{\sigma\to\omega} \tag{55}$$

$$= \sum_{\alpha\beta}\chi^\sigma_{\alpha\beta}\ |\omega_\alpha\rangle\rangle_\sigma\langle\langle\omega_\beta|_\sigma \tag{56}$$

where the superscripts σ, ω denote the basis of the χ-matries. This is illustrated in Fig. 33.

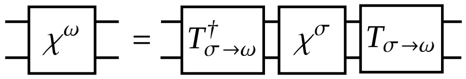

FIG. 33. Tensor network for changing a process matrix χ^σ with respect to basis $\{\sigma_\alpha\}$ to a process matrix χ^ω with respect to basis $\{\omega_\alpha\}$.

IV. TRANSFORMING BETWEEN REPRESENTATIONS

We now proceed to the task of describing how one may transform between representations of completely-positive trace-preserving maps, as depicted in Fig. 1. In particular, the transformations depicted as solid arrows in Fig. 1 have succinct descriptions in the graphical calculus we introduced in Section II. These transformations are based on the wire bending dualities for reshuffling, vectorization, and the Choi-Jamiołkowski isomorphism. While the remaining transformations depicted as dashed lines are not based on dualities, but rather non-linear decompositions, or constructions, they also have diagrammatic representations in our graphical calculus for completely positive maps.

A. Transformations between the Choi-matrix and superoperator representations

The Choi-matrix and superoperator are naturally equivalent under the reshuffling wire bending duality introduced in Section II A. In the col (row) convention we may transform between the two by applying the bipartite col (row)-reshuffling operation R introduced in Section II A. Let $\Lambda \in \mathcal{L}(\mathcal{X}\otimes\mathcal{Y})$ be the Choi-matrix, and $\mathcal{S} \in \mathcal{L}(\mathcal{X}\otimes\mathcal{X}\mathcal{Y}\otimes\mathcal{Y})$ be the superoperator, for a map $\mathcal{E}\in\mathcal{T}(\mathcal{X},\mathcal{Y})$. Then we have

$$\Lambda = S^R \qquad \mathcal{S} = \Lambda^R \tag{57}$$

This is illustrated in Fig. 34. In terms of tensor components we have

$$\Lambda_{mn,\mu\nu} = \mathcal{S}_{\nu n,\mu m} \tag{58}$$

where m, n and μ, ν index the standard bases for $\mathcal{X}$ and $\mathcal{Y}$ respectively.

Graphical proofs of the relations $\Lambda^{R_c} = \mathcal{S}$ and $\mathcal{S}^{R_c} = \Lambda$ are given in Fig.s 35 and 36 respectively.

To transfer between a process matrix with respect to an arbitrary operator basis, and a superoperator with respect to an arbitrary vectorization basis, we must first convert both to col-vec (or row-vec) convention and then proceed by reshuffling.

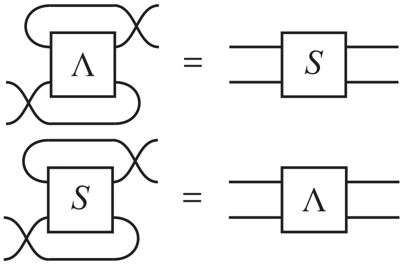

FIG. 34. Transforations between superoperator and Choi matrix are done by the wire bending duality for the bipartite reshuffling operation (Fig. 15f).

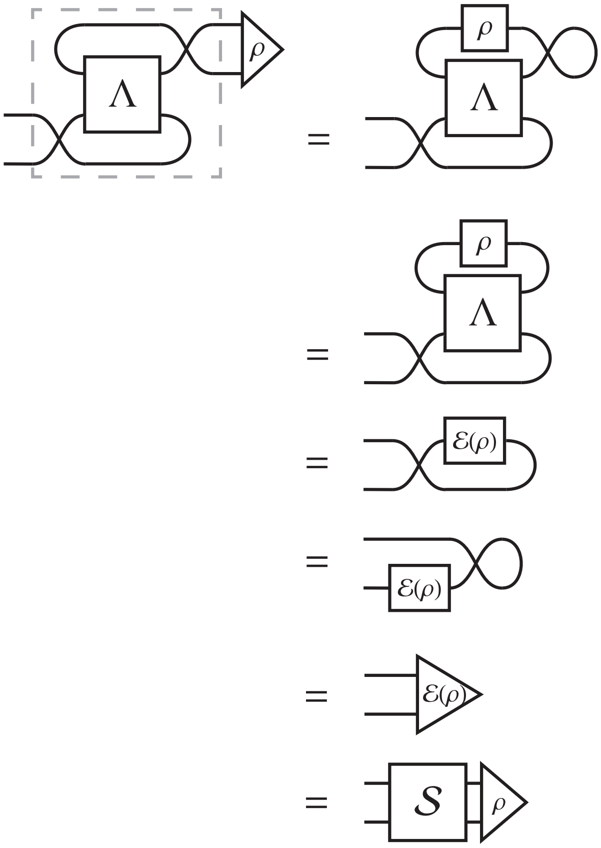

FIG. 35. Graphical proof that the reshuffled Choi-matrix Λ^R satisfies the evolution equation for the superoperator representation (27).

Note that reshuffling is it's own inverse, ie $(\Lambda^R)^R = \Lambda$, hence the solid bi-directional arrow connecting the Choi-matrix and superoperator representations in Fig. 1. This is the only transformation between the representations we consider which is linear, bijective, and self-inverse.

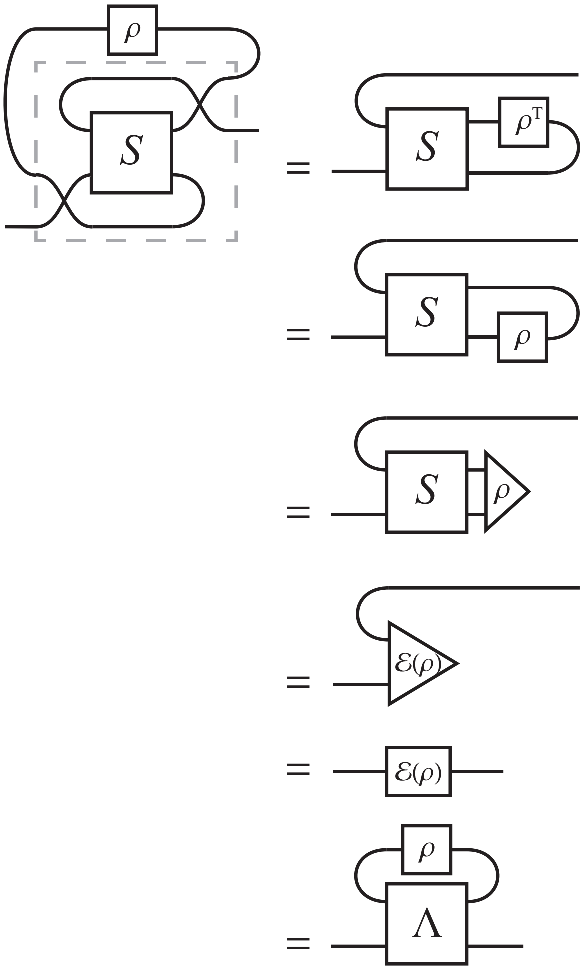

FIG. 36. Graphical proof that the reshuffled superoperator $\mathcal{S}^R$ satisfies the evolution equation for the Choi-matrix representation (42).

B. Transformations to the superoperator representation

Transformations to the superoperator from the Kraus and system-environment representations of a CP-map are also accomplished by a wire-bending duality, in this case vectorization. However, unlike the bijective equivalence of the Choi-matrix and superoperator under the reshuffling duality, the vectorization duality is only surjective.

If we start with a Kraus representation for a CPTP map $\mathcal{E} \in \mathcal{C}(\mathcal{X}, \mathcal{Y})$ given by $\{K_\alpha : \alpha = 0, ..., D-1\}$, with $K_\alpha \in \mathcal{L}(\mathcal{X}, \mathcal{Y})$, we can construct the superoperator $\mathcal{S} \in \mathcal{L}(\mathcal{X} \otimes \mathcal{X}, \mathcal{Y} \otimes \mathcal{Y})$ by

$$\mathcal{S} = \sum_{\alpha=0}^{D-1} \overline{K}_\alpha \otimes K_\alpha. \tag{59}$$

The corresponding tensor network is given in Fig. 37 and the graphical proof of this relationship follows directly from Roth's lemma and is found in Fig. 38.

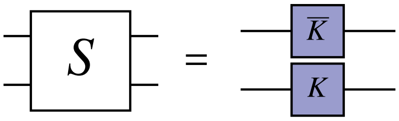

FIG. 37. Tensor network for constructing the superoperator representation $\mathcal{S}$ for a CPTP-map $\mathcal{E}$ from a Kraus representation $\{K_\alpha : \alpha = 0, \dots D-1\}$.

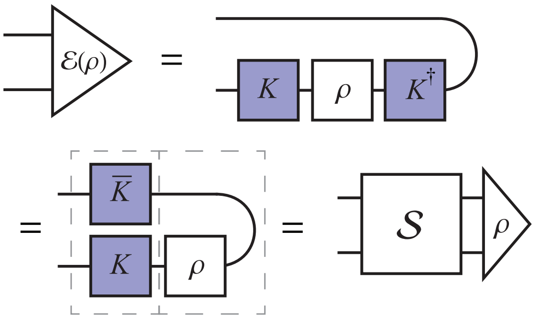

FIG. 38. Graphical proof asserting the validity of Eqn (59) for constructing a superoperator representation $\mathcal{S}$ from a Kraus representation $\{K_\alpha\}$.

Starting with a system-environment (or Stinespring) representation with a map $\mathcal{E} \in \mathcal{C}(\mathcal{X}, \mathcal{Y})$ with system Hilbert space $\mathcal{X} \cong \mathbb{C}^d$ and environment Hilbert space $\mathcal{Z} \cong \mathbb{C}^D$ with $1 \le D \le \dim(\mathcal{L}(\mathcal{X}, \mathcal{Y}))$, we may construct the superoperator for this map from the joint system-environment unitary U and initial environment state $|v_0\rangle$ by

$$\mathcal{S} = \sum_\alpha \langle\alpha|\overline{U}|v_0\rangle \otimes \langle\alpha|U|v_0\rangle, \tag{60}$$

where $\{|\alpha\rangle : \alpha = 0, ..., D-1\}$ is an orthonormal basis for $\mathcal{Z}$. The corresponding tensor network is given in Fig. 39. As with the Kraus to superoperator transformation, the proof of Eqn (60) follows from Roth's lemma.

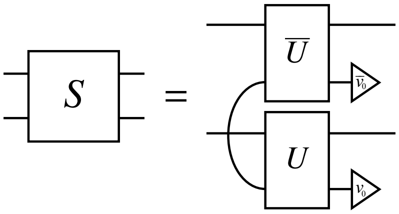

FIG. 39. Tensor network for constructing the superoperator representation $\mathcal{S}$ for a CPTP-map $\mathcal{E}$ from a System-Environment representation with initial environment state $|v_0\rangle$ and joint unitary U.

Note that while the vectorization wire bending duality is invertible, these transformations to the superoperator from the Kraus and system-environment representations are single directional. In both cases injectivity fails as the superoperator is unique, while both the Kraus and system-environment representations are not. Hence we have solid single directional arrows in Fig. 1 connecting both the Kraus and system-environment representations to the superoperator. The inverse transformation from a superoperator to the Kraus or system-environment representation requires a canonical decomposition of the operator $\mathcal{S}$ (via first reshuffling to the Choi-matrix), which is detailed in Sections IV D and IV E.

C. Transformations to the Choi-matrix representation

Transforming to the Choi-matrix from the Kraus and system-environment representations is accomplished via a wire-bending duality which captures the Choi-Jamiołkowski isomorphism. As with the case of transforming to the superoperator, this duality transformation is surjective but not injective.

Given a set of Kraus matrices $\{K_\alpha : \alpha = 0, ..., D-1\}$ where $K_\alpha \in \mathcal{L}(\mathcal{X}, \mathcal{Y})$ for a CPTP-map $\mathcal{E} \in \mathcal{C}(\mathcal{X}, \mathcal{Y})$, one may form the Choi-Matrix Λ as was previously illustrated in Fig. 28 in Section III D. In terms of both Dirac notation and tensor components we have:

$$\Lambda = \sum_{i,j} \left(|i\rangle\langle j| \otimes \sum_\alpha K_\alpha |i\rangle\langle j| K_\alpha^\dagger \right) \tag{61}$$

$$= \sum_\alpha |K_\alpha\rangle\rangle\langle\langle K_\alpha| \tag{62}$$

$$\Lambda_{mn,\mu\nu} = \sum_\alpha (K_\alpha)_{\mu m} (\overline{K}_\alpha)_{\nu n}. \tag{63}$$

where $\{|i\rangle\}$ is an orthonormal basis for $\mathcal{X}$, m, n index the standard basis for $\mathcal{X}$, and μ, ν index the standard basis for $\mathcal{Y}$.

Given a system-environment representation with joint unitary $U \in \mathcal{L}(\mathcal{X}, \mathcal{Z})$ and initial environment state $|v_0\rangle \in \mathcal{Z}$ we have

$$\Lambda = \sum_{i,j} \left(|i\rangle\langle j| \otimes \mathrm{Tr}_{\mathcal{Z}} \left[U|i\rangle\langle j| \otimes |v_0\rangle\langle v_0| U^\dagger \right] \right) \tag{64}$$

This is shown graphically in Fig. 40.

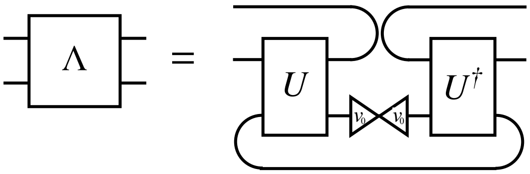

FIG. 40. Construction of the Choi-matrix representation Λ from a system-environment representation with initial environment state $|v\rangle$ and joint unitary U via the Choi-Jamiołkowski isomorphism (40).

The proof of these transformations follow directly from the definition of the Choi-matrix in Eqn (38), and the tensor networks for the evolution via the Kraus or system-environment representations given in Figues 23 and 24 respectively. As with the vectorization transformation to the superoperator discussed in Section IV B, even though the Choi-Jamiołkowski isomorphism is linear these transformations are single directional as injectivity fails due to the non-uniqueness of both the Kraus and system-environment representations. Hence we have the solid single-directional arrows connecting both the Kraus and system-environment representations to the Choi-matrix in Fig. 1.

This completes our description of the linear transformations between the representations of CP-maps in Fig. 1. We will now detail the non-linear transformations to the Kraus and system environment representations.

D. Transformations to the Kraus Representation

We may construct a Kraus representations from the Choi-matrix or system-environment representation by the non-linear operations of spectral-decomposition and partial trace decomposition respectively. To construct a Kraus representation from the Superoperator however, we must first reshuffle to the Choi-matrix.

To construct Kraus matrices from a Choi matrix we first recall the graphical Spectral decomposition we introduced as an example of our colour summation convention in Section II. If $\mathcal{E}$ is CP by Eqn (48) we have $\Lambda_{\mathcal{E}} \geq 0$ and hence the spectral decomposition of the Choi-matrix is given by

$$\Lambda_{\mathcal{E}} = \sum_{\alpha} \lambda_{\alpha}^2 |\phi_\alpha\rangle\langle\phi_\alpha|, \tag{65}$$

where $\lambda_\alpha \geq 0$. Hence we can define Kraus operators $K_\alpha = \lambda_\alpha A_\alpha$ where A_α is the unique operator satisfying $|A_\alpha\rangle\rangle = |\phi_\alpha\rangle$ as illustrated in Fig. 41. The number of Kraus operators will be equal to the rank r of the Choi-matrix, where $1 \leq r \leq \dim(\mathcal{L}(\mathcal{X},\mathcal{Y}))$. The graphical proof of this transformation is given in Fig. 42. The proof that Kraus operators satisfy the completeness relation follows from the trace preserving property of Λ in Eqn (46). This is given in Fig. 43.

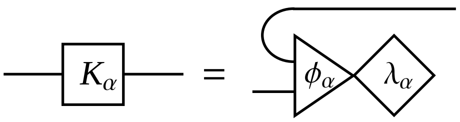

FIG. 41. Construction of a Kraus representation K_α for a CPTP-map $\mathcal{E}$ from the Choi-matrix representation Λ by the de-vectorization of the spectral decomposition of the Choi-matrix $\Lambda = \sum_\alpha \lambda_\alpha^2 |\phi_\alpha\rangle\langle\phi_\alpha|$.

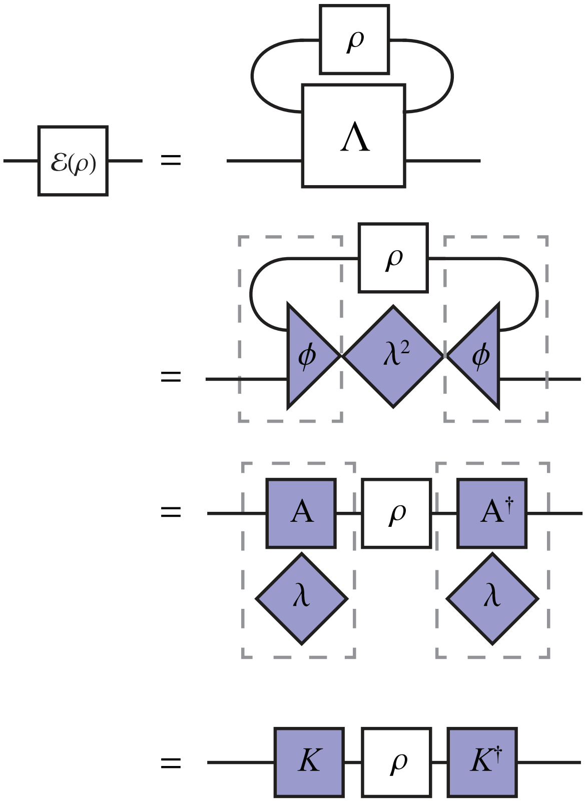

FIG. 42. Graphical proof of Fig. 41 for the construction of a Kraus representation $\{K_\alpha\}$ for a CPTP-map $\mathcal{E}$ from the Choi-matrix representation Λ.

Note that since Λ, and the χ-matrix are related by a unitary change of basis, the Kraus representations constructed from their respective spectral decompositions will also be related by the same transformation. Each will give a unitarily equivalent Canonical Kraus representation of $\mathcal{E}$ since the eigen-vectors are orthogonal. Thus we have described the arrow in Fig. 1 connecting the Choi-matrix to the Kraus representation. It is represented as a dashed arrow as it involves a non-linear decomposition, and is single directional as this representation transformation is injective, but not surjective. Surjectivity fails as we can only construct the canonical Kraus representations for $\mathcal{E}$. The reverse transformation is given by the Jamiołkowski isomorphism described in Section IV C.

Starting with a system-environment representation with joint unitary $U \in \mathcal{L}(\mathcal{X},\mathcal{Z})$ and initial environment state $|v_0\rangle \in \mathcal{Z}$, we first choose an orthonormal basis $\{|\alpha\rangle : \alpha = 0, ..., D-1\}$ for $\mathcal{Z}$. We then construct the Kraus representation by decomposing the partial trace

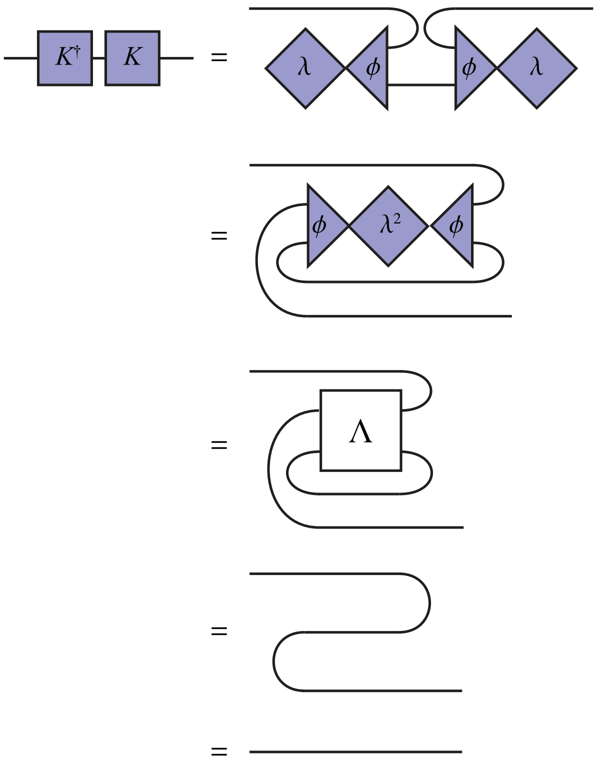

FIG. 43. Graphical proof of the completeness relation (23) for the Kraus representation $\{K_\alpha\}$ constructed from the Choi-matrix representation as given in Fig. 41. This follows from the trace preserving property of the Choi-matrix representation (47).

in this basis as follows

$$\mathcal{E}(\rho) = \mathrm{Tr}_E\left[U\left(\rho\otimes|v\rangle\langle v|\right)U^\dagger\right] \tag{66}$$

$$= \sum_{\alpha=0}^{D-1}\langle\alpha|U|v_0\rangle\rho\langle v_0|U^\dagger|\alpha\rangle \tag{67}$$

$$= \sum_{\alpha=0}^{D-1} K_\alpha\rho K_\alpha^\dagger \tag{68}$$

A sequence of tensor contractions illustrating the validity of this results are given in Fig. 45. Hence we may define Kraus matrices

$$K_\alpha = \langle\alpha|U|v_0\rangle \tag{69}$$

leading to the tensor network given in Fig. 44.

Though the Kraus and system-environment representations are both non-unique, for a fixed basis for the environment this partial trace decomposition is an injective transformation between the Kraus and Stinespring representations (or equivalently between the Kraus and system-environment representations when the joint unitary is restricted to a fixed initial state of the environment). To see let $\{K_\alpha\}$ and $\{J_\alpha\}$ be two Kraus representations constructed from Stinespring representations

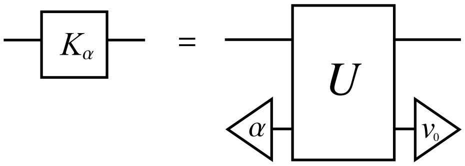

FIG. 44. Construction of a Kraus representation $\{K_j : \alpha = 0,\ldots,D-1\}$ from a system-environment representation with initial environment state $|v_0\rangle$, joint unitary U, and an orthonormal basis for the environment $\{|\alpha\rangle : \alpha = 0,\ldots,D-1\}$.

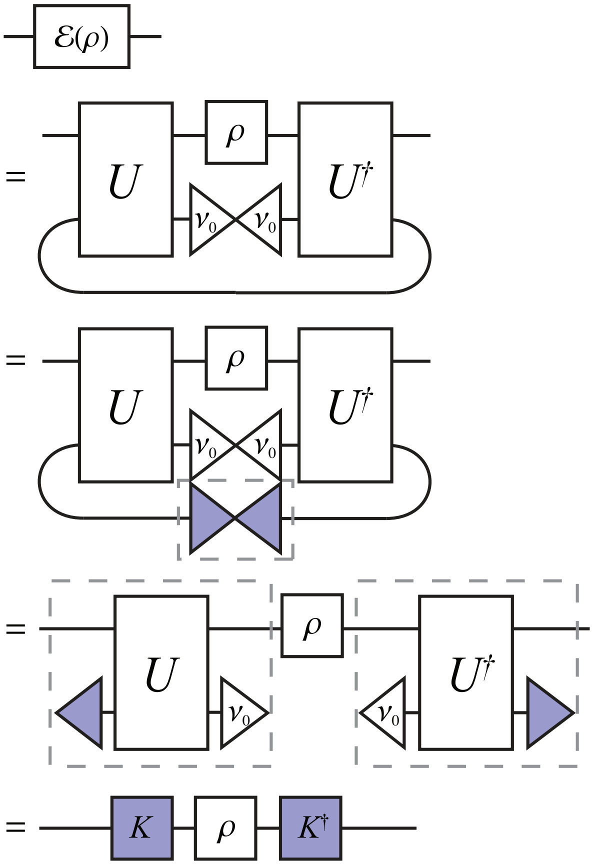

FIG. 45. Graphical proof Proof of Fig. 44 for constructing a Kraus representation $\{K_\alpha\}$ from a system environment representation with initial environment state $|v_0\rangle$ and joint unitary U.

A and B respectively for a CPTP-map $\mathcal{E} \in \mathcal{C}(\mathcal{X},\mathcal{Y})$. Then we have that

$$K_\alpha = J_\alpha \tag{70}$$

$$\Leftrightarrow (K_\alpha)_{ij} = (J_\alpha)_{ij} \tag{71}$$

$$\Leftrightarrow A_{i\alpha,j} = B_{i\alpha,j} \tag{72}$$

$$\Leftrightarrow A = B. \tag{73}$$

Since the Stinespring operators satisfy $A = U|v_0\rangle$ and $B = V|v_0\rangle$ for some joint unitaries U and V, we must have that $U_0 = V_0$ where U_0 and V_0 are the joint unitaries restricted to the subspace of the environment spanned by $|v_0\rangle$.

This transformation can be thought of as the reverse application of the Stinespring dilation theorem, and hence for a fixed choice of basis (and initial state of the environment) it is invertible. The inverse transformation is the Stinespring dilation, and as we will show in Section IV E, since the inverse transformation is also injective this transformation is a bijection. However, since the partial trace decomposition involves a choice of basis for the environment it is non-linear — hence we use a dashed bi-directional arrow to represent the transformation from the system-environment representation to the Kraus representation in Fig. 1.

E. Transformations to the system-environment representation

We now describe the final remaining transformation given in Fig. 1, the bijective non-linear transformation from the Kraus representation to the system-environment, or Stinespring, representation. The system-environment representation is the most cumbersome to transform to since it is it involves the unitary completion of a Stinespring dilation of a Kraus representation. Thus from a Superoperator one must first reshuffle to the Choi-matrix, and form the Choi-matrix description one must then spectral decompose to the canonical Kraus representation before finally constructing the system-environment as follows.

Let $\{K_\alpha : \alpha = 0, ..., D-1\}$ where $1 \leq D \leq \dim(\mathcal{L}(\mathcal{X}, \mathcal{Y}))$, be a Kraus representation for the CP-map $\mathcal{E} \in \mathcal{T}(\mathcal{X}, \mathcal{Y})$. Consider an ancilla Hilbert space $\mathcal{Z} \cong \mathbb{C}^D$, this will model the environment. If we choose an orthonormal basis for the environment, $\{|\alpha\rangle : \alpha = 0, ..., D-1\}$, then by Stinesprings dilation theorem we may construct the Stinespring matrix for the CP map $\mathcal{E}$ by

$$A = \sum_{\alpha=0}^{D-1} K_\alpha \otimes |\alpha\rangle. \tag{74}$$

Recall from Section III B that the Stinespring representation is essentially the system-environment representation when the joint unitary operator is restricted to the subspace spanned by the initial state of the environment. Hence if we let $|v_0\rangle \in \mathcal{H}_E$ be the initial state of the environment system, then this restricted unitary is given by

$$U_0 = \sum_\alpha K_\alpha \otimes |\alpha\rangle\langle v_0|, \tag{75}$$

as illustrated in Fig. 46. The graphical proof of this construction giving the required evolution of a state ρ can be found in Fig. 47. In principle, one may complete the remaining entries of this matrix to construct the full matrix description for the unitary U, however such a process is cumbersome and is unnecessary to describe the evolution of the CP-map $\mathcal{E}$ [17].

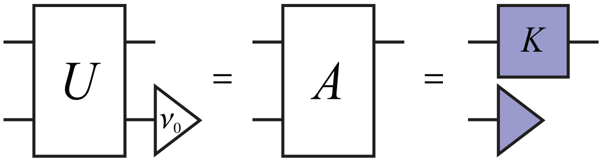

(a) Stinespring operator

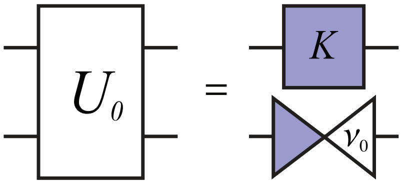

(b) Restricted unitary

FIG. 46. Construction of a Stinespring representation A and system-environment representation with initial environment state $|v_0\rangle$ and joint unitary U for a CPTP-map $\mathcal{E}$ from a Kraus representation $\{K_\alpha\}$. Note that U_0 is the restriction of the joint unitary U to the subspace of the environment spanned by the initial state $|v_0\rangle$.

Hence we have finished characterizing the final transformations depicted in Fig. 1 connecting the Kraus representation to the system-environment representation by Stinespring dilation. As previously mentioned in Section IV D, for a fixed choice of basis for the environment, and initial state of the environment, the transformation between Kraus and Stinespring representations is bijective (and hence so is the transformation between Kraus and system-environment representations when restricted to the subspace spanned by the initial state of the environment). Though both these representations are non-unique, by fixing a basis and initial state for the environment we ensure that this transformation is injective. To see this let U_0 and V_0 be unitaries restricted to the state $|v_0\rangle$ constructed from Kraus representations, $\{K_\alpha\}$ and $\{J_\alpha\}$ respectively, for $\mathcal{E} \in \mathcal{C}(\mathcal{X}, \mathcal{Y})$. Then

$$U_0 = V_0 \Leftrightarrow \sum_\alpha K_\alpha \otimes |\alpha\rangle\langle v_0| = \sum_\alpha J_\alpha \otimes |\alpha\rangle\langle v_0| \tag{76}$$

$$\Leftrightarrow \sum_\alpha K_\alpha \langle\beta|\alpha\rangle = \sum_\alpha J_\alpha \langle\beta|\alpha\rangle \tag{77}$$

$$\Leftrightarrow K_\beta = J_\beta \tag{78}$$

Bijectivity then follows from the injectivity of the inverse transformation — the previously given construction of a Kraus representation by the partial trace decomposition of a joint unitary operator in Fig. 44.

V. CONCLUSION

The study of completely-positive trace-preserving maps is an old topic, so it is perhaps surprising that

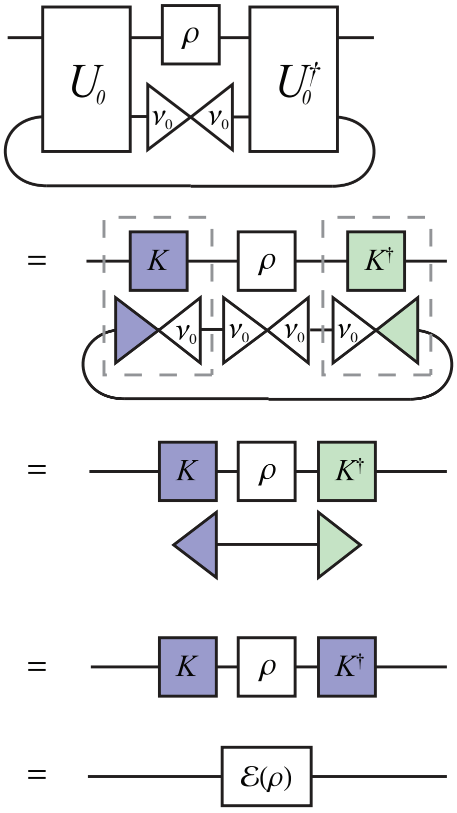

FIG. 47. Graphical proof that the restricted unitary U_0 constructed from a Kraus representation by (75) gives the correct description of CP map $\mathcal{E}$.

there are still new insights to be gained by investigating their structure using new techniques. Further, while the application of CPTP-maps to describing the evolution of open quantum systems is well understood, it is a surprisingly difficult task to find a concise summary of the properties of, and transformations between, their various mathematically equivalent representations used in the quantum information processing literature. The graphical calculus for open quantum systems presented in this paper has enabled us to unify, and hence transform freely between, the various common representations of CPTP-maps by performing diagrammatic manipulations of their respective tensor networks. A summary of these transformations between the different representations was given in Fig. 1.

We found that many of these transformations between representations of CPTP-maps corresponded to wire bending dualities in our graphical calculus, which have a particularly succinct tensor network description. These transformations are depicted by solid arrows between two boxes labelling representations in Fig. 1. Of these duality transformations, only the reshuffling operation connecting the Choi-matrix and Liouville-superoperator is bi-directional — the reshuffling operation is bijective and self-inverse, and hence the same transformation takes the Choi-Matrix to the superoperator as takes the superoperator to the Choi-matrix. The two other wire bending dualities are vectorization, which transforms both the Kraus and system-environment representations to the superoperator representation, and the Choi-Jamiołkowski isomorphism, which transforms the same two representations to the Choi-matrix. These duality transformations are only single directional as they are not injective, and hence depicted by a one-way arrow connecting the appropriate boxes labelling these representations in Fig. 1. The reason these transformations are single directional, as apposed to the bi-directional transformation between the Choi-matrix and superoperator, is due to the non-uniqueness of the Kraus and system-environment representations of a CPTP-map. The transformation is a many-to-one (surjective) mapping and not strictly invertible without first specifying some form of decomposition of the superoperator or Choi-matrix.

The transformations we presented for transitioning from the Choi-matrix to the Kraus representation, and between the Kraus and system-environment representations, were not based solely on wire bending dualities. These transformations are depicted by dashed arrows in Fig. 1, where the dash is meant to indicate that they are non-linear transformations. This non-linearity arose from the decompositions and constructions involved, for example the spectral decomposition of a positive-semi definite operator in the Choi-matrix to Kraus representation transformation. In our case, these non-linear transformations were all also one directional due to the non-uniqueness of the representation being transformed to. There is unitary freedom in constructing them — for the Choi-matrix to Kraus representation transformation, one could change the basis of the eigenvectors with respect to a vectorization convention and still arrive at a valid Kraus representation; for Kraus to the system environment representation one may choose any orthonormal basis in the construction of the joint system-environment unitary in Eqn (75); and for the system environment to Kraus representation one may decompose the partial trace over the environment in any orthonormal basis.

Having new tools to investigate old problems can often lead to surprising new results, and we believe there are many potential applications in QIP for the graphical calculus we have presented in this paper.

VI. ACKNOWLEDGEMENTS

This work was supported by the Canadian Excellence Research Chairs (CERC) Program and the Canadian Institute for Advanced Research (CIFAR). JDB completed part of this work while visiting Michele Mosca at IQC.

[1] M. A. Nielsen and I. L. Chuang, *Quantum Computation and Quantum Information* (Cambridge University Press, 2000).
[2] R. Penrose, Combinatorial Mathematics and its Applications, Academic Press (1971).
[3] J. C. Baez and A. Lauda, arXiv:hep-th/0908.2469 (2009), 0908.2469.
[4] J. D. Biamonte, S. R. Clark, and D. Jaksch, to appear, AIP Advances, arXiv:quant-ph/1012.0531 (2010).
[5] V. Bergholm and J. D. Biamonte, J. Phys. A: Math. Theor. **44**, 245304 (2011).
[6] G. Vidal, Phys. Rev. Lett. **101**, 110501 (2008).
[7] G. Evenbly and G. Vidal, Phys. Rev. B **79**, 144108 (2009).
[8] F. Verstraete, V. Murg, and J. Cirac, Advances in Physics **57**, 143 (2008).
[9] S. Abramsky and B. Coecke, A categorical semantics of quantum protocols, in *Proceedings of the 19th Annual IEEE symposium on Logic in Computer Science*, p. 21, IEEE Computer Society Press, 2004, 0402130.
[10] S. Abramsky, arXiv:quant-ph/0910.2737A (2009).
[11] G. Chiribella, G. M. D'Ariano, and P. Perinotti, Phys. Rev. A **84**, 012311 (2011).
[12] L. Hardy, arXiv:quant-ph/1103.2066 (2011).
[13] P. Selinger, A survey of graphical languages for monoidal categories, in *New Structures for Physics*, , Lecture Notes in Physics Vol. 813, pp. 289–355, Springer Berlin, 2011.
[14] P. Selinger, Electronic Notes in Theoretical Computer Science **170**, 139 (2007).
[15] R. A. Horn and C. R. Johnson, *Matrix Analysis* (Cambridge Uni. Press, Cambridge, 1985).
[16] K. Kraus, *States, Effects and Operations: Fundamental Notions of Quantum Theory*, Lecture Notes in Physics Vol. 190 (Springer, Berlin, 1983).
[17] I. Bengtsson and K. Życzkowski, *Geometry of Quantum States* (Cambridge University Press, Cambridge, 2006).
[18] W. Stinespring, Positive functions on C*-algebras, in *Proc. Amer. Math. Soc*, pp. 211–216, 1955.
[19] Y. S. Weinstein *et al.*, The Journal of Chemical Physics **121**, 6117 (2004).
[20] H. A. Carteret, D. R. Terno, and K. Życzkowski, Phys. Rev. A **77**, 042113 (2008).
[21] C. J. Wood, Non-completely positive maps: Properties and applications, Master's thesis, Macquarie University, 2008.
[22] M.-D. Choi, Linear Algebrra Appl. **10** (1975).
[23] A. Jamiołkowski, Reports on Mathematical Physics **3**, 275 (1972).
[24] G. D'Ariano and P. Lo Presti, Phys. Rev. Lett. **91** (2003).
[25] J. Altepeter *et al.*, Phys. Rev. Lett. **90** (2003).

Appendix A: Tensor networks

We will now prove the consistency of several of the basic tensor networks introduced in Section II, and in doing so illustrate how one may use our graphical calculus for diagrammatic reasoning.

The colour summation convention we have presented represents diagrammatic summation over a tensor index by colouring the appropriate tensors in the diagram. In this convention summation over a Kronecker delta is as shown in Fig. 48. This expression is used in several of the following proofs.

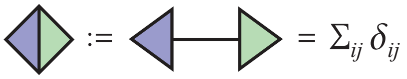

FIG. 48. Colour summation convention for $\sum_{i,j}\langle i|j\rangle = \sum_{i,j}\delta_{ij}$. Multiplication of a tensor network by this quantity converts all diagrams with either of the two colours present in the left hand side, to the same colour.

We begin with the proof of the trace of an operator A which is given in Fig. 49.

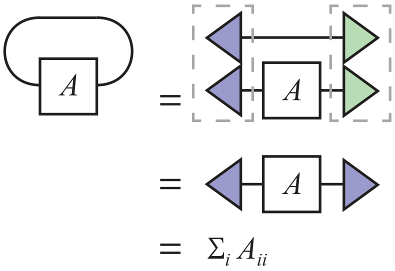

FIG. 49. Proof that our tensor network for graphical trace does return $\mathrm{Tr}(A) \equiv \sum_i A_{ii}$.

For illustrative purposes, to prove this algebraically we note that the tensor networks for trace correspond to the algebraic expressions $\langle\Phi^+|A\otimes\mathbb{1}|\Phi^+\rangle$ and $\langle\Phi^+|\mathbb{1}\otimes A|\Phi^+\rangle$, and that

$$\langle\Phi^+|A\otimes\mathbb{1}|\Phi^+\rangle = \sum_{i,j}\langle i|A|j\rangle\langle i|j\rangle \tag{A1}$$

$$= \sum_{i,j}\delta_{ij}A_{ij} \tag{A2}$$

$$= \sum_{i}A_{ii} \tag{A3}$$

$$= \mathrm{Tr}[A]. \tag{A4}$$

Similarly we get $\langle\Phi^+|\mathbb{1}\otimes A|\Phi^+\rangle = \mathrm{Tr}[A]$.

To prove the snake equation we must first make the following equivalence for tensor products of the elements $|i\rangle$ and $\langle j|$:

$$\langle j|\otimes|i\rangle \equiv |i\rangle\otimes\langle j| \equiv |i\rangle\langle j| \tag{A5}$$

This is illustrated diagrammatically in Fig. 50.

With this equivalence made, the proof of the snake-equation for the "S" bend is given in Fig. 51. The proof for the reflected "S" snake-equation follows naturally from the equivalence defined in Fig. 50.

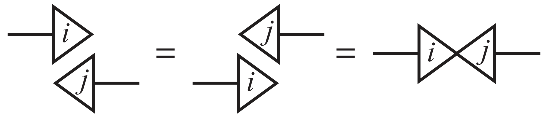

FIG. 50. Equivalence of tensor product expressions $|i\rangle\otimes\langle j|, \langle j|\otimes|i\rangle, |i\rangle\langle j|$.

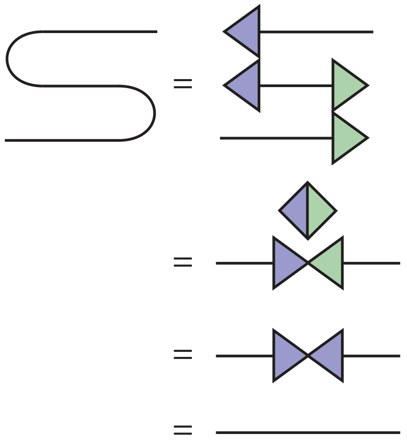

FIG. 51. Graphical proof of the snake equation.

The proof of our tensor network for the transposition of a linear operator A is shown in Fig. 52. To prove this algebraically we note that the corresponding algebraic equation for the transposition tensor network is

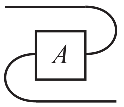

$$= \mathbb{1}\otimes\langle\Phi^+|(\mathbb{1}\otimes A\otimes\mathbb{1})|\Phi^+\rangle\otimes\mathbb{1} \tag{A6}$$

$$= \sum_{i,j}\langle j|A|i\rangle\ |i\rangle\otimes\langle j| \tag{A7}$$

$$= \sum_{i,j}\langle j|A|i\rangle|i\rangle\langle j| \tag{A8}$$

$$= \sum_{i,j}\langle i|A^T|j\rangle|i\rangle\langle j| \tag{A9}$$

$$= \sum_{i,j}|i\rangle\langle i|A^T|j\rangle\langle j| \tag{A10}$$

$$= A^T. \tag{A11}$$

The proof for transposition by counter-clockwise wire bending follows from the equivalence relation in Eqn (A5).

With the tensor network for transposition of an operator proven, the proof of transposition by contracting through a Bell-state $|\Phi^+\rangle$ is then an application of the snake-equation as shown in Fig. 53.

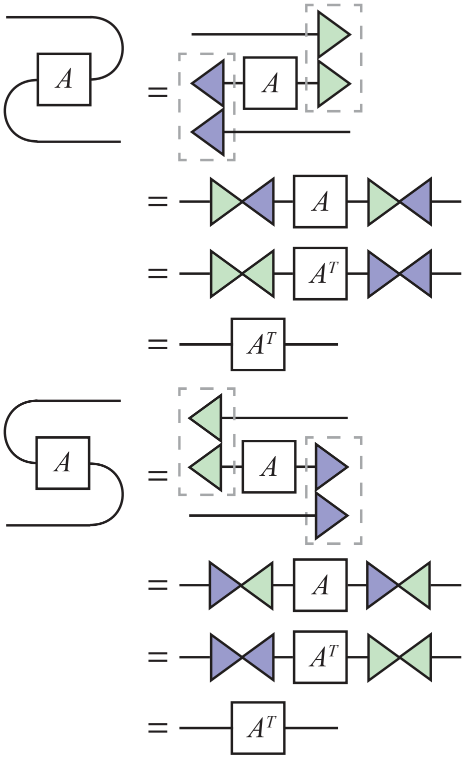

FIG. 52. Proof of transposition tensor network.

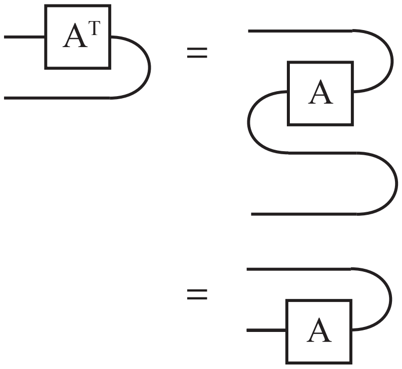

FIG. 53. Proof of transposition by "sliding".

Appendix B: Vectorization change of basis

We now prove that the vectorization change of basis operator $T_{\sigma\rightarrow\omega}$ indeed functions as claimed. Let $\mathcal{H}$ be a d-dimensional complex Hilbert space and let $\{\sigma_\alpha : \alpha = 0, ..., d^2-1\}, \{\omega_\alpha : \alpha = 0, ..., d^2-1\}$ be orthonormal operator bases for $\mathcal{L}(\mathcal{H})$. Define an operator $T_{\sigma\rightarrow\omega}\in\mathcal{L}(\mathcal{H}\otimes\mathcal{H})$ by

$$T_{\sigma\rightarrow\omega} := \sum_\alpha |\alpha\rangle\langle\langle\omega_\omega|_\sigma. \tag{B1}$$

where $\{|\alpha\rangle : \alpha = 0, d^2-1\}$ is the computational basis for $\mathcal{H}\otimes\mathcal{H}$.

We claim that for any linear operator $A \in \mathcal{L}(\mathcal{H})$,

$$T_{\sigma\to\omega}|A\rangle\rangle_\sigma = |A\rangle\rangle_\omega. \tag{B2}$$

The proof is as follows:

$$\begin{aligned} T_{\sigma\to\omega}|A\rangle\rangle_\sigma &= \left(\sum_\alpha |\alpha\rangle\langle\langle\omega_\alpha|_\sigma\right)|A\rangle\rangle_\sigma & \text{(B3)} \\ &= \sum_\alpha |\alpha\rangle\langle\langle\omega_\alpha|A\rangle\rangle_\sigma & \text{(B4)} \\ &= \sum_\alpha |\alpha\rangle \operatorname{Tr}[\omega_\alpha^\dagger A] & \text{(B5)} \\ &= |A\rangle\rangle_\omega. & \text{(B6)} \end{aligned}$$

The inverse of $T_{\sigma\to\omega}$ is given by

$$T_{\sigma\to\omega}^{-1} = T_{\sigma\to\omega}^\dagger = T_{\omega\to\sigma} \tag{B7}$$

and hence $T_{\sigma\to\omega}$ is unitary.